Ultrafast reaction dynamics of the associative hydrogen desorption from Ru(001)

2008 J. Phys.: Condens. Matter 20 313002

(http://iopscience.iop.org/0953-8984/20/31/313002)

J. Phys.: Condens. Matter **20** (2008) 313002 (22pp) doi:10.1088/0953-8984/20/31/313002

TOPICAL REVIEW

Ultrafast reaction dynamics of the associative hydrogen desorption from Ru(001)

Christian Frischkorn

Freie Universität Berlin, Fachbereich Physik, Arnimallee 14, D-14195 Berlin, Germany

E-mail: christian.frischkorn@physik.fu-berlin.de

Received 18 February 2008, in final form 30 April 2008
Published 17 July 2008
Online at stacks.iop.org/JPhysCM/20/313002

Abstract

For a microscopic understanding of chemical reactions at surfaces, it is essential to obtain detailed knowledge on the underlying elementary processes. The reaction mechanism, the pathways and timescales of energy flow and the energy partitioning between different degrees of freedom of the reaction products are of key interest. Reactions of species adsorbed on a metal surface are generally mediated through electron and/or phonon excitations of the substrate. Since thermal equilibration between these excitations occurs on a femto- to picosecond timescale, chemical reactions initiated by ultrashort laser pulses provide the base to investigate processes beyond equilibrium conditions. The recombination of two hydrogen atoms forming an H_2 molecule, which leaves the surface, represents one of the most basic surface reactions one could think of and thus may serve as a prototype system for femtosecond laser-induced surface chemistry. In particular, the $H_{ads} + H_{ads} \rightarrow H_{2,gas}$ associative desorption from a Ru(001) surface has been studied in great detail. Ultrafast energy transfer times of less than 200 fs in conjunction with a pronounced isotope effect between H_2 and D_2 unambiguously indicate a hot-substrate electron-driven reaction mechanism. Measurements of the energy partitioning between external (translational) and internal (vibrational, rotational) degrees of freedom of the product molecule reveal predominantly translational excitation of the desorbing hydrogen. Theoretical modelling based on a multidimensional frictional description of energy transfer between the ruthenium substrate and the hydrogen layer excellently reproduces the experimental findings. Furthermore, peculiar characteristics like a threshold-like coverage dependence of the desorption yield and promotion effects in isotopically substituted adlayers have been observed in the experiment which demonstrate the importance of strong adsorbate–adsorbate interactions in the H_2/D_2 association, yet still awaiting a quantitative theoretical treatment.

(Some figures in this article are in colour only in the electronic version)

Contents

1. Introduction 2
2. Basic concepts in surface femtochemistry 3
   2.1. Excitation and energy flow within the substrate 3
   2.2. Substrate–adsorbate energy transfer 4
3. Experimental approaches to ultrafast surface reactions 7
   3.1. Optical pump–mass spectrometry probe 7
   3.2. State-resolved detection 10
   3.3. Vibrational spectroscopy 11
4. Hydrogen association from Ru(001) 11
   4.1. Excitation mechanism of fs-laser-driven reaction 12
   4.2. Adsorbate–adsorbate interactions 14
   4.3. Energy partitioning 16
   4.4. Multidimensional dynamics 18
5. Concluding remarks 20
Acknowledgments 21
References 21

1. Introduction

Inducing and controlling surface reactions by light has been a long-standing goal in surface science. While in early attempts, thermal activation upon light absorption may have often been the dominant mechanism [1], non-thermal photochemistry at surfaces was established only in the late 1980s [2, 3]. In these experiments, usually nanosecond (ns) (or continuous-wave (cw)) laser excitation was employed to induce processes like desorption, dissociation and reactions of molecules adsorbed at metal or semiconductor surfaces. One common observation was a *linear* dependence of the reaction yield on the number of absorbed photons by the substrate. These findings could only be rationalized by a non-thermal excitation mechanism which invokes a *single* electronic transition between the ground and an excited potential energy surface (PES). For most systems studied, the electronic excitation step has been attributed to attachment of photoexcited substrate electrons to an unoccupied adsorbate resonance (e.g. the LUMO (lowest unoccupied molecular orbital) level) [1, 2]. The corresponding excitation mechanism in these surface photochemistry reactions is frequently called—in analogy to electron stimulated desorption processes—desorption induced by electronic transitions (DIET) [4].

The first experiments using femtosecond (1 fs $= 10^{-15}$ s) laser pulses were performed by Heinz and coworkers, who reported a novel non-thermal desorption mechanism for NO/Pd(111) under fs-laser excitation with a highly nonlinear fluence dependence of the reaction yield [5]. Furthermore, when the desorption process was induced by a pair of time-delayed fs-laser pulses in a two-pulse correlation scheme, a sub-picosecond response time was obtained [6]. These findings could only be explained by a mechanism which invokes nonadiabatic coupling between the fs-laser excited electron–hole pair distribution in the substrate and the adsorbate vibrational degrees of freedom as the driving force for the chemical reaction [7, 8]. Thereby, absorption of a fs-light pulse by a metal substrate generates a transient non-equilibrium distribution of hot electrons, which thermalize by ultrafast electron–electron scattering and lead to an electron temperature exceeding the lattice temperature by several thousand degrees kelvin on a sub-picosecond timescale [9]. Coupling of this electronic transient to adsorbate vibrational degrees of freedom will eventually cause chemical processes which include desorption [5, 10], diffusion [11, 12] or reactions between coadsorbed species [13–16]. Since these reactive processes compete with various energy dissipation channels to the electronic and phononic degrees of freedom of the underlying substrate, the reaction dynamics occur predominantly on the ground state PES. Conceptually, the coupling mechanism into the adsorbate vibrational degree of freedom (the reaction coordinate) can be either described as desorption induced by *multiple* electronic transitions (DIMET) between two diabatic PESs [17] or by nonadiabatic electron–nuclear coupling via electronic friction [18].

Surface femtochemistry, i.e. chemical reactions at the surface initiated by fs-laser pulses, has attracted increasing attention since the first reports in 1990 [8]. This is especially due to the fact that coupling between electronic and nuclear degrees of freedom as an almost ubiquitous phenomenon in photoinduced processes in physics and chemistry is inherent to surface femtochemistry at metals: the initially photoexcited electrons of the metal substrate lead to nuclear motions of the adsorbates. Femtosecond-laser excitation of a metal allows us to directly study the timescales of energy flow between the electronic and lattice excitations of the substrate and the adsorbate (vibrational) degrees of freedom. Such a process violates the Born–Oppenheimer approximation and thus provides a test case for nonadiabatic coupling processes at metal surfaces in a quantitative manner. A further appealing characteristic of surface femtochemistry is the access to this nonadiabatic coupling in the time domain which allows us to 'switch on' electronic frictional forces by ultrashort laser pulses. Such an excitation may therefore serve as an ultrafast trigger for real-time studies of surface reaction dynamics [12]. Moreover, the ability to bring the reactants into close proximity in a well-defined adsorption state provides additional control of the reaction dynamics, e.g. in associative desorption reactions triggered by fs-laser pulses [14, 19].

The field of surface femtochemistry is strongly connected to other surface science areas where nonadiabaticity plays a crucial role like vibrational energy relaxation at metal surfaces [20] or mode-selective chemistry induced by inelastic tunnelling or by the electric field in a scanning tunnelling microscope (STM) [21, 22]. Further particularly striking examples of nonadiabatic coupling between electronic and nuclear degrees of freedom are gas–surface interactions where in exothermic adsorption at metal surfaces electron–hole pair excitation in the substrate leads to chemicurrents, chemiluminescence or even exoelectron emission [23]. These kinds of nonadiabatic processes in adsorption can be regarded (at least in part) as the time reversal of the DIET or DIMET processes in desorption reactions and challenge theoretical concepts, which frequently rely on the validity of the Born–Oppenheimer approximation [24].

Reactive processes at surfaces are of fundamental importance for technological applications such as heterogeneous catalysis [26]. There, metals are often investigated as model substrates since the interaction of the adsorbed reaction partners with the substrate may cause a favourable energy landscape, e.g. a reduced reaction barrier compared to the gas phase as sketched in figure 1 for a generic associative desorption of a diatomic molecule. In particular, hydrogen and its interaction with transition-metal surfaces has attracted significant attention in both experimental and theoretical work on, for instance, catalytic reactions [26] and hydrogen storage in metals [27]. Fundamental research on hydrogen at surfaces has been carried out to address a variety of different aspects like H-induced surface reconstruction [28, 29], substrate-mediated interaction between coadsorbed H atoms [19, 30] and quantum delocalization [31, 32], which might impose additional complexity of the adsorbate–substrate system despite the structural simplicity of the adsorbate.

The present work focuses on the associative desorption of hydrogen from a ruthenium (001) surface induced by ultrashort laser pulses. The recombination of two hydrogen

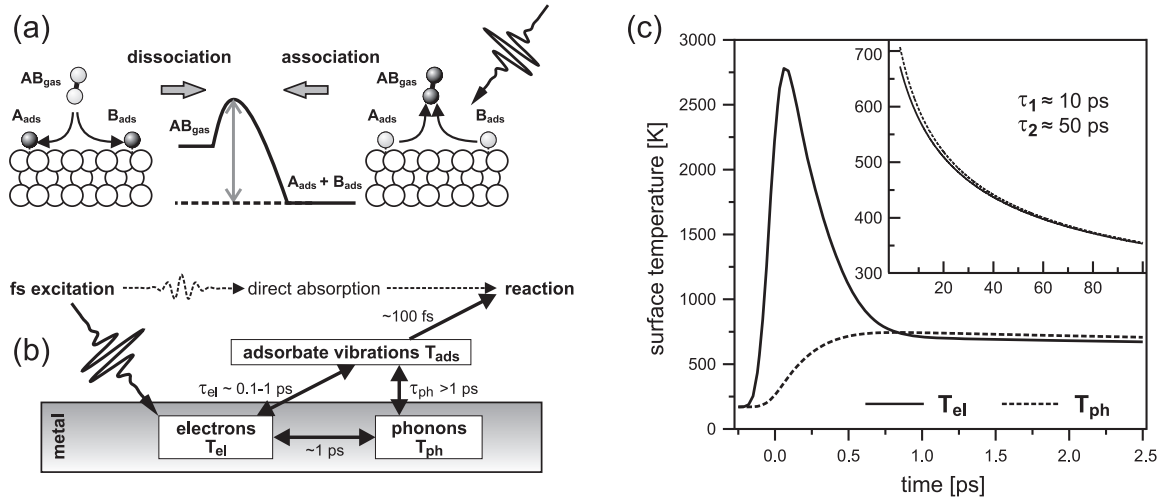

Figure 1. (a) Sketch of a diatomic dissociation and association reaction, respectively. The key aspect of the presented experiments described here is to trigger the back reaction, the associative desorption of the adsorbed atomic species by an ultrashort laser pulse. (b) Energy flow after femtosecond-laser excitation of a metal surface based on a coupled heat bath model for electrons and phonons with respective temperatures T_{el} and T_{ph} describing the energy content of the metal substrate and the adsorbate characterized by a third temperature T_{ads}. Typical coupling times between the various heat baths are given. Reaction is initiated either by direct adsorption (however, usually negligible in thin atomic or molecular layers) or indirectly by energy transfer from the substrate to the adsorbate. After sufficient energy is accumulated in a relevant adsorbate coordinate, the reaction may occur. Reproduced with permission from [25]. Copyright 2002 World Scientific Publishing Co. Pte. Ltd, Singapore. (c) Typical temperature transients for the electron and phonon heat baths calculated with the two-temperature model [9] here for ruthenium as the metal substrate at a base temperature of 170 K. The parameters of the exciting laser pulse are 130 fs and 60 J m^{-2} at a centre wavelength of 800 nm. After the initially strong thermal non-equilibrium between electrons and phonons, both subsystems equilibrate within the electron–phonon coupling time. Subsequently, electrons and phonons cool down largely simultaneously (with T_{ph} somewhat larger than T_{el}, see text) with time constants of several tens of ps (biexponential fit yields two relaxation times of 10 and 50 ps, respectively).

atoms desorbing into the gas phase may also occur through conventional thermal heating of the Ru substrate, but if initiated by fs-laser excitation distinct characteristics are observed. A comprehensive set of experimental and theoretical results have been obtained leading to a detailed picture of the dynamics in the $H_{ads} + H_{ads} \rightarrow H_{2,gas}$ reaction. In the following, an overview of the basic concepts of surface femtochemistry will be given first, followed by the experimental techniques available to investigate the ultrafast dynamics of surface reactions. In the main part, the results on the fs-laser-induced hydrogen association reaction will be grouped into four sections; (i) the excitation mechanism, (ii) the adsorbate–adsorbate interactions, (iii) the energy partitioning between different degrees of freedom of the reaction product and (iv) the multidimensional frictional description of the reaction dynamics. In the final concluding remarks, an forecast will be given on what challenges and potential future work remain for surface femtochemistry in general and in particular for the H/Ru(001) system.

2. Basic concepts in surface femtochemistry

In surface femtochemistry, the processes initiated by the ultrashort laser pulse excitation of the absorbate-covered metal surface can be divided into two parts [8]. The first field covers processes within the substrate where the laser pulse is absorbed and the energy dissipated, since substrate-mediated reactions typically dominate (i.e. direct optical absorption is mostly negligible in atomically thin adsorbate layers). The second field comprises the subsequent energy transfer to the adsorbate system which involves the coupling of electronic and nuclear degrees of freedom. Figure 1(b) illustrates the primary excitation process together with the subsequent energy flow between the different subsystems. Characteristic time constants for the respective energy transfer are given. In the following subsection, the processes of intrasubstrate and substrate–adsorbate energy transfer are expanded in more detail.

2.1. Excitation and energy flow within the substrate

From a simplified point of view, a metal substrate consists of two heat baths; the ion cores (lattice) and the surrounding electron gas. Excitations of either of these subsystems, i.e. collective lattice vibrations (phonons) and electron gas excitations respectively, constitute the energy content of the substrate. Consequently, the degree of excitation can be described by two population distributions, each characterized (in the limit of thermalized distributions) by a temperature T_{el} or T_{ph} for the electron and phonon subsystem, respectively (see figure 1(b)). In thermal equilibrium or when the substrate is heated conventionally (i.e. not by ultrafast laser excitation), equal temperatures for both heat baths prevail; $T_{el} = T_{ph}$ due to electron–phonon coupling with a typical equilibration time in the few picosecond (ps) range. However, excitation with a femtosecond-laser pulse will drive the system out of equilibrium (figure 1(c)). The pulse energy is deposited into the electron system and, due to the small heat capacity of the electrons compared to the lattice, T_{el} rises within the pulse

Table 1. Relevant input data for the two-temperature model calculations for ruthenium comprising physical material constants and optical properties.

Property	Symbol	Value	Units	Ref
Electronic heat capacity	γ_{el}	400	J m^{-3} K^{-2}	[37]
Electronic thermal conductivity	κ_0	117	W m^{-1} K^{-1}	[37]
Debye temperature	θ_D	404	K	[38]
Electron–phonon coupling constant	g	1.85×10^{18}	W m^{-3} K^{-1}	[39]
Refractive index (800 nm)	$n_r + i\,n_i$	$5.04 + i\,3.94$		[40]
Refractive index (400 nm)	$n_r + i\,n_i$	$2.40 + i\,4.64$		[40]
Optical penetration depth (800 nm)	δ	16.2	nm	
Optical penetration depth (400 nm)	δ	6.9	nm	
Reflectivity (800 nm)	R	61.3	%	
Reflectivity (400 nm)	R	71.0	%	

width to levels far above the melting point of the lattice. This electronic excitation energy is then dissipated either by electron diffusion into the bulk or by energy transfer into the phonon subsystem via electron–phonon coupling. This gives rise to an increase of the phonon temperature T_{ph}, however, on a much slower timescale than the electronic response. Within a time span of approximately the electron–phonon coupling time of the substrate, both the electron and phonon heat bath equilibrate. The so-called two-temperature model (2TM) has been established to quantitatively describe such a system of two coupled heat baths. Figure 1(c) shows typical temperature transients $T_{el}(t)$ and $T_{ph}(t)$ for the electrons and phonons, respectively, obtained with the 2TM demonstrating the strong thermal non-equilibrium between both heat baths within the first picosecond after laser excitation (in the case of ruthenium as the metal). Subsequently, on a few ps to several hundreds of ps timescale, both systems relax virtually simultaneously, however, with a slightly lower temperature for the electrons. This fact that $T_{el}(t) > T_{ph}(t)$ for $t > t_{eq}$ after the 'initial' thermalization ($T_{el}(t_{eq}) = T_{ph}(t_{eq})$) originates from thermal electronic diffusion, by which the electrons cool the phonon bath.

Mathematically, the 2TM is represented by the following coupled differential equations [9, 33]:

$$C_{el}\frac{\partial}{\partial t}T_{el} = \overbrace{\frac{\partial}{\partial z}\kappa_{el}\frac{\partial}{\partial z}T_{el}}^{\text{therm. diffusion}} - \overbrace{g(T_{el}-T_{ph})}^{\text{el-ph coupling}} + \overbrace{S(z,t)}^{\text{opt. excitation}} \quad (1)$$

$$C_{ph}\frac{\partial}{\partial t}T_{ph} = +g(T_{el}-T_{ph}). \quad (2)$$

Here, $C_{el} = \gamma T_{el}$ and C_{ph} are the electron and ion heat capacities, respectively. $\kappa_{el} = \kappa_0 T_{el}/T_{ph}$ is the electronic thermal conductivity and g is the electron–phonon coupling constant. Heat conduction by phonons can be neglected in metals due to the fact that the respective mean velocities of electrons and phonons enter the heat conductivity quadratically (note that in metals the Fermi velocity exceeds the speed of sound by far). The term $S(z,t)$ finally describes the optical excitation of the electrons and can be expressed by [34]

$$S(z,t) = \frac{(1-R)I(t)}{\delta}\cdot\exp(-z/\delta), \quad (3)$$

where δ, R and $I(t)$ stand for the optical penetration depth, the substrate reflectivity and the time profile of the laser intensity, respectively. Details on the electron and lattice dynamics following ultrafast optical excitation of metals can be found, for instance, in [35, 36]. Table 1 summarizes the relevant physical properties of ruthenium used in the two-temperature model calculations for the description of the experimental hydrogen recombination data further below.

2.2. Substrate–adsorbate energy transfer

The two energy reservoirs of the substrate, i.e. the electron and phonon subsystem, respectively, may couple energy independently into the adsorbate system. After accumulation of sufficient energy in the coordinate relevant to a certain reaction, the adsorbate may undergo desorption, dissociation or reactions between coadsorbed species (see figure 1(b)). The energy transfer from the initially excited electronic degrees of freedom of the substrate to the nuclear motion of the reactants occurs either directly through electronically nonadiabatic substrate–adsorbate coupling or indirectly via equilibration with the lattice and subsequent coupling to the adsorbate, whereby energy is transferred adiabatically in the electronic ground state via successive ladder climbing (figure 2(a)). In order to describe these energy transfer mechanisms in surface femtochemistry, two conceptually different frameworks have been developed.

One substrate–adsorbate coupling scenario, which accounts only for purely electron-mediated excitation processes, invokes 'desorption (or, more generally, dynamics) induced by multiple electronic transitions' (DIMET) [17]. In such a DIMET process as illustrated in figure 2(b), hot-substrate electrons transiently populate a normally unoccupied affinity level transferring the absorbate–substrate complex to an electronically excited PES, which can be either anti-bonding, i.e. repulsive, as in the Menzel–Gomer–Redhead (MGR) [41, 42] picture or bonding as proposed by Antoniewicz [43]. The new charge distribution resulting from the transient electron transfer initiates nuclear motion converting potential energy into kinetic energy. After relaxation back to the electronic ground state, the system has acquired vibrational energy. At high excitation densities, additional excitation/deexcitation cycles might occur before vibrational energy relaxation takes place on the ground state PES, thus enabling the adsorbate to accumulate sufficient energy in the relevant coordinate to overcome the reaction barrier.

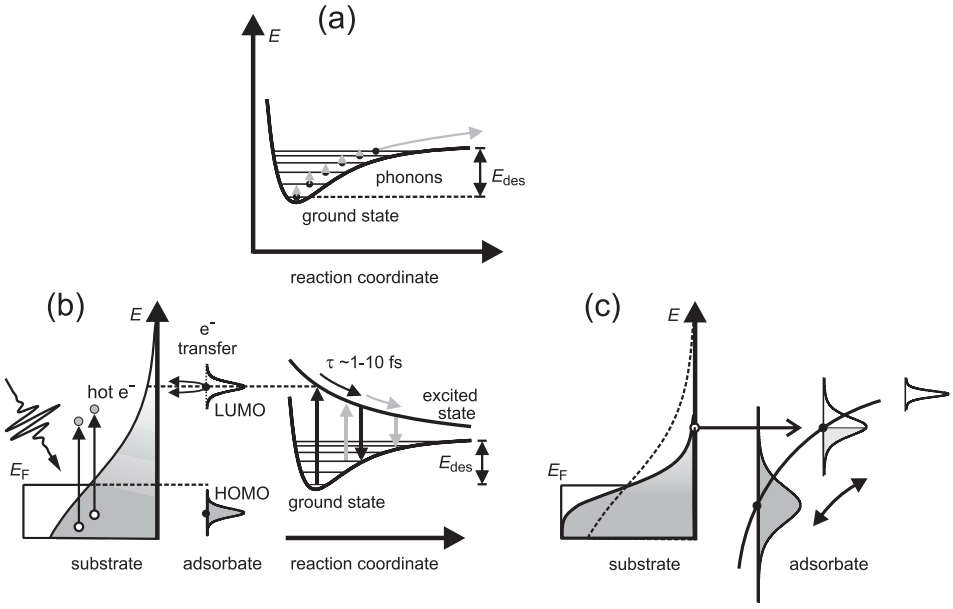

Figure 2. Illustration of substrate–adsorbate coupling mechanisms. (a) Phonon mediation of a surface reaction proceeding adiabatically on the electronic ground state via vibrational ladder climbing. (b) DIMET picture of electron mediation involving (multiple) electronic transitions: the high-energy tail of the electronic occupation distribution transiently populates unoccupied molecular orbitals of the adsorbate–substrate complex (e.g. the LUMO). After relaxation back to the ground state, vibrational energy has been acquired and accordingly repeated excitation/deexcitation cycles lead to desorption. (c) Frictional picture of electron-driven energy transfer. An adsorbate-derived affinity level broadens and may be transiently populated by substrate electrons as the adsorbate moves towards the metal surface. Friction ('resistance') damps the evolving electron flow back and forth between the substrate and the adsorbate resonance. Note that a high-lying adsorbate resonance can only be populated by substrate electrons of a hot electronic distribution (as indicated by the dashed line), while at lower temperatures such a resonance remains unaccessible. Panels (a), (b) adapted from [25], panel (c) adapted from [8].

The second approach treats the energy transfer in terms of frictional forces between either of the substrate's subsystems (electron and phonons) and the adsorbate [44, 45] with respective frictional coefficients[1] $\eta_{el} = 1/\tau_{el}$ and $\eta_{ph} = 1/\tau_{ph}$. These coefficients determine how fast energy flows into the adsorbate system. In the reverse process of vibrational energy relaxation, these coupling times can be interpreted as the vibrational lifetime (T_1) and are therefore connected to the lifetime contribution to the IR linewidth of the respective vibration [20, 46]. The origin of electronic friction can be explained within the Anderson–Newns model [47], whereby an adsorbate-derived affinity level shifts downwards and broadens for decreasing adsorbate–substrate distances (figure 2(c)). If such a level is transiently populated by substrate electrons the charge-induced adsorbate motion results in a level shift as the adsorbate starts moving along the corresponding reaction coordinate. Electron flow back and forth between the metal substrate and the adsorbate is intrinsically affected by damping, i.e. friction. To which extent adsorbate levels might be populated depends on the electronic temperature of the substrate (see figure 2(c)). Usually low-lying energy levels are involved in excitations via electronic friction. While in the friction picture, *high*-lying substrate–adsorbate resonances might not be reached, those levels might well be populated in a DIMET process to induce nuclear motion by electrons from the high-energy tail of a hot Fermi–Dirac distribution (or by electrons not yet thermalized directly after photoexcitation).

[1] η_{el} is related to the friction coefficient γ of a classical velocity-proportional friction force $F = -\gamma v$ by $\eta_{el} = \gamma/m$ with m being the adsorbate mass [18].

The two concepts (DIMET and friction model) incorporate similar physical processes in a different mechanistic description. While in the DIMET model, the adsorbate transiently resides in an electronically excited PES which induce forces on the nuclei, in the frictional description of substrate–adsorbate coupling the adsorbate resonances are filled 'nearly' adiabatically with substrate electrons, which exert fluctuating forces on the nuclei, leading to chemistry. In the latter scenario, the adsorbate remains in the ground PES, in contrast to the DIMET approach. These seemingly contradictory theoretical descriptions of ultrafast laser-induced surface chemistry are simply based on two different representations to solve the breakdown of the Born–Oppenheimer approximation that causes this kind of femtochemistry, with the DIMET model based on the diabatic representation and the electronic friction approach based on the adiabatic representation [48, 49]. Note that at high excitation densities, as is the case in surface femtochemistry with multiple electronic transitions between the ground and excited state PES, both the DIMET and the friction scenario are physically equivalent, whereby the DIMET process corresponds to a strongly temperature-dependent friction coefficient in the electronic friction picture. A unifying formalism is given in [45].

For a quantitative theoretical description of the energy transfer from the laser-excited substrate to the reactants in the adsorbate layer in surface femtochemistry processes, usually the frictional coupling approach has been applied (e.g. [11, 12, 15, 19, 44, 50]). Thereby, the heat baths of the substrate, electrons and phonons, are connected to a harmonic

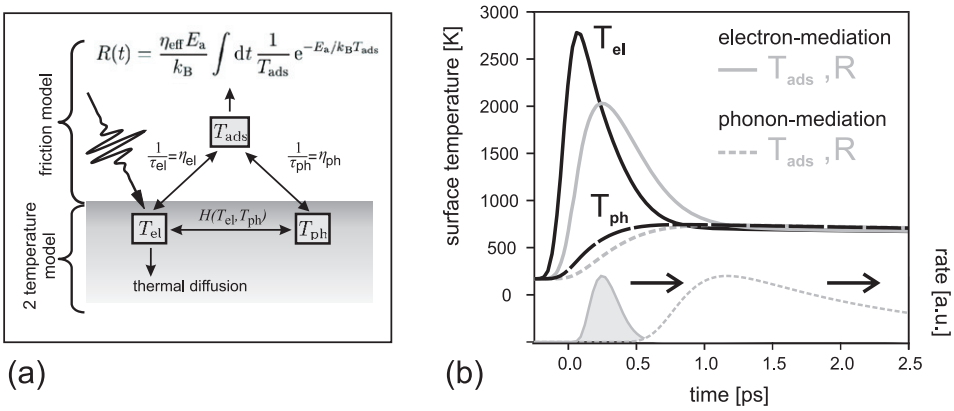

Figure 3. Modelling the energy flow within the metal substrate and from the substrate to the adsorbate. (a) Schematic of the two-temperature model for the electron and phonon subsystems of the substrate in conjunction with frictional coupling to the adsorbate heat bath. Energy dissipation of the initially excited electrons takes place either via heat diffusion into the bulk of the substrate or via electron–phonon coupling represented by the coupling term $H(T_{el}, T_{ph})$. The latter is frequently used in the simplified form [33, 54, 55] $H(T_{el}, T_{ph}) = g(T_{el} + T_{ph})$, with g as the electron–phonon coupling constant of equations (1) and (2). (b) Typical temperatures transients for femtosecond laser excitation of a metal substrate: here, in particular, ruthenium (Ru) excited with a pulse of 130 fs in duration and an absorbed fluence of $F = 60$ J m^{-2} (calculated with the 2TM using material constants and optical properties of Ru as listed in table 1). Furthermore, the adsorbate temperature T_{ads} and the normalized reaction rate R are calculated for a purely electron- and a purely phonon-mediated energy transfer scenario both with the same value for the coupling time $\tau_{el} = 180$ fs and $\tau_{ph} = 180$ fs, respectively, and an activation energy E_a of 1.35 eV.

oscillator of the adsorbate motion via frictional coefficients η_{el} and η_{ph} which determine the coupling strength (see figure 3(a)). Based on a master equation formalism [18], the time evolution of the energy content of the adsorbate is represented by [44, 50]

$$\frac{d}{dt}U_{ads} = \eta_{el}(U_{el} - U_{ads}) + \eta_{ph}(U_{ph} - U_{ads}), \qquad (4)$$

with the Bose–Einstein distributed mean vibrational energy

$$U_x = \frac{h\nu_{ads}}{e^{h\nu_{ads}/k_B T_x} - 1} \qquad (5)$$

of an oscillator at temperature T_x, $x =$ el and ph, respectively. ν_{ads} refers to the frequency of the vibration along the reaction coordinate. In this so-called empirical friction model accounting for both electronic and phononic contributions, the adsorbate temperature T_{ads} is obtained by solving equation (4) with T_{el} and T_{ph} computed in the two-temperature model, see equations (1) and (2). The reaction rate R and, finally, to compare with the experiment, the reaction yield Y as the time integral of R are calculated with an Arrhenius-type expression

$$R(t) = -\frac{d}{dt}\theta(t) = \theta^n(t)\, k_0\, e^{-E_a/k_B T_{ads}(t)}, \qquad (6)$$

where θ and n denote the coverage and the order of the reaction kinetics, respectively. As an alternative, a modified friction model has been proposed by Brandbyge *et al* [45], in which a purely electronic frictional coupling is incorporated. Here, the frictional force originates from coupling of Langevin noise of the electron heat bath (T_{el}) into the adsorbate centre-of-mass coordinate (represented by T_{ads}). Based on the same master equation as in the former case, one obtains the adsorbate temperature T_{ads} by solving

$$\frac{d}{dt}T_{ads}(t) = \eta_{el}(t)[T_{el}(t) - T_{ads}(t)]. \qquad (7)$$

Equation (7) can be formally derived from the high-temperature limit of equation (4) (with electronic contributions only) if $h\nu_{ads}/k_B T_x \ll 1$ and therefore $U_x \approx k_B T_x$. In principle, η_{el} depends on time and space and has to be calculated by microscopic theories [46, 51, 52], see section 4.4. The rate in this modified electronic friction model scales proportionally with the reaction probability which in turn depends on a Boltzmann factor in a similar way as in the empirical model:

$$R(t) \propto P_{rxn} = E_a \int_0^\infty dt\, \frac{\eta_{el}}{T_{ads}(t)}\, e^{-E_a/k_B T_{ads}(t)}. \qquad (8)$$

However, in contrast to equation (6), the friction coefficient η_{el}, T_{ads} and the energy E_a enter the pre-exponential factor. Taking into account the mass dependence of the friction coefficient $\eta_{el} \propto 1/m$, the Brandbyge model [45] directly leads to an isotope effect in the reaction yield for isotopically substituted reactants in contrast to the empirical model discussed above. It should be noted that within both frictional models the energy E_a is the well depth of a truncated one-dimensional harmonic oscillator. However, it turns out that values for E_a extracted from experimental data typically exceed the measured activation energies for desorption. Initially, it has been speculated that E_a should be regarded as a modified activation energy which is larger than the depth of the adsorption well, indicating the population of electronically excited states [19]. This is, however, not consistent with the original assumption of the frictional models. Thus, it appears more likely, in particular for association reactions, that the multidimensionality of the relevant PES which governs the reaction dynamics is the origin of the discrepancy between the values for E_a derived from the friction calculations and those experimentally obtained from thermally induced reactions [53], see also section 4.4. Phase space constraints imposed through the projection of the multidimensional

motion onto a single coordinate cause an additional barrier that adds to the true energy for desorption [53].

To illustrate the inherent difference in timescales between electron- and phonon-mediated energy transfer channels, figure 3(b) shows model calculations for both scenarios. Depending on whether substrate electrons or phonons couple energy into the adsorbate system via friction, the adsorbate temperature T_{ads} rises with a certain time delay to the 'driving' heat bath T_{el} or T_{ph}. Note that, even with identical coupling times of each of the metal subsystems with the adsorbate layer, the reaction rate and hence the yield of an *electron*-mediated process is observed on a sub-picosecond timescale within a rather narrow temporal window of a few 100 fs. In contrast, in the case of a *phonon*-driven energy transfer, the reaction occurs significantly later and is widely stretched in time over several ps. The time difference between the onset of an electron- versus a phonon-mediated reaction is further increased when phonon coupling times in the ps range are taken which are more realistic for an energy transfer process dominated by phonons, as observed in the experiment; see, for instance, [34].

3. Experimental approaches to ultrafast surface reactions

In general, surface femtochemistry experiments are performed by applying amplified fs-laser pulses to well-defined metal/adsorbate systems in ultrahigh vacuum (UHV). While laser fluences up to several 100 J m^{-2} (close to the damage threshold of the substrate) are necessary to realize a chemical reaction to a substantial extent, UHV base pressures of typically $<1 \times 10^{-10}$ mbar in conjunction with standard surface science tools are required for preparation and characterization of the substrate and the adsorbed reactants.

In the following subsections, the main experimental techniques available to investigate ultrafast photoinduced surface reactions, and in particular the associative hydrogen desorption from ruthenium, will be described. In optical pump–mass spectrometry probe techniques, the mass signal of the desorption products is measured after the sub-picosecond pump pulse has triggered the reaction. Various excitation parameters may be varied like the laser fluence and wavelength, or the excitation is applied via a pulse sequence as in a two-pulse correlation scheme. Furthermore, the starting reaction system might be altered by isotopic substitution or different adsorbate coverages. To identify peculiarities of a fs-laser-induced reaction in comparison to the reaction initiated under thermal equilibrium conditions (which is possible for the $H_{ads} + H_{ads} \rightarrow H_{2,gas}$ reaction on Ru(001)), thermal desorption spectroscopy (TDS) is employed. In a second class of experiments, the desorbing product species are not only detected as successful reaction events, but state selectively via resonance-enhanced multiphoton ionization (REMPI). To this end, the femtosecond laser set-up needs to be synchronized to a tunable excitation laser. Besides scanning the wavelength, the polarization of the resonant excitation step might also be changed in the detection process, providing information on the state population and the motion of the nascent reaction product particles. Finally, time-resolved all-optical pump–probe studies exploit an optically induced product-specific system response as a function of the time delay between pump and probe pulses. In such experiments, typically surface-sensitive vibrationally resonant sum-frequency generation (SFG) is used, whereby the vibrational signature serves as a monitor for the evolving reaction dynamics.

3.1. Optical pump–mass spectrometry probe

Successfully performing surface femtochemistry experiments (especially association and desorption reactions) relies on sufficiently high fluences (see above) of the exciting laser at a spot size (typically a few mm in diameter) on the adsorbate-covered sample large enough for mass detection of the desorbing product species. This requires pulse energies in the few mJ range, while pulse lengths of ∼100–150 fs are still adequate to study processes which involve chemical bond breaking and formation with corresponding timescales of a molecular vibrational period. In particular for the experiments on the H/Ru system presented in this review, a high-power laser system comprising a Ti:sapphire oscillator with regenerative and multipass amplification stages (Quantronix, Titan II) has been used which delivers fs-laser pulses of typically 130 fs in duration with pulse energies of up to 4.5 mJ at 800 nm centre wavelength. The repetition rate may be adjusted from 400 Hz down to 20 Hz using a pulse picker between the amplification stages; single-shot experiments are performed by the additional aid of a chopper and/or shutters. The pulse energy and hence the incident fluence can be varied by adjusting the pump power of the Nd:YLF lasers to the multipass amplifier. However, this also changes the thermal load to the multipass stage/compressor unit and leads to different overall beam characteristics which in turn directly affects the fluence F of the excitation. A more advantageous method for fluence-dependent studies is to vary the transmission of the laser output through a combination of $\lambda/2$ plates and a thin-film polarizer at otherwise constant operational parameters of the amplifier.

As will be shown further below, precise pulse characterization is of crucial importance in surface femtochemistry, since the yield of a fs-laser-induced surface reaction is usually non-linearly dependent on the absorbed fluence (see figure 12). To this end, a reference beam channel is used in which the beam profile is detected by a CCD (charge-coupled device) camera at a position equivalent to the sample under UHV (figure 4). Possible self-focusing distortions imposed by the entrance window into the UHV chamber at high laser fluences are accounted for by placing a reference window with a similar self-focusing behaviour into the reference pathway. Furthermore, although ruthenium has a rather high optical damage threshold ($F_{thres} > 250$ J m^{-2} [16]), the fluences used in the experiment might be still high enough to bear the risk of ablation. However, this can minimized by a reference Ru crystal also placed outside the chamber into one arm of the pulse characterization channel.

The actual sample for the associative hydrogen desorption experiments, a Ru(001) single crystal, is mounted in a UHV chamber on a liquid helium cooled cryostat which, in conjunction with resistive heating, enables temperature control

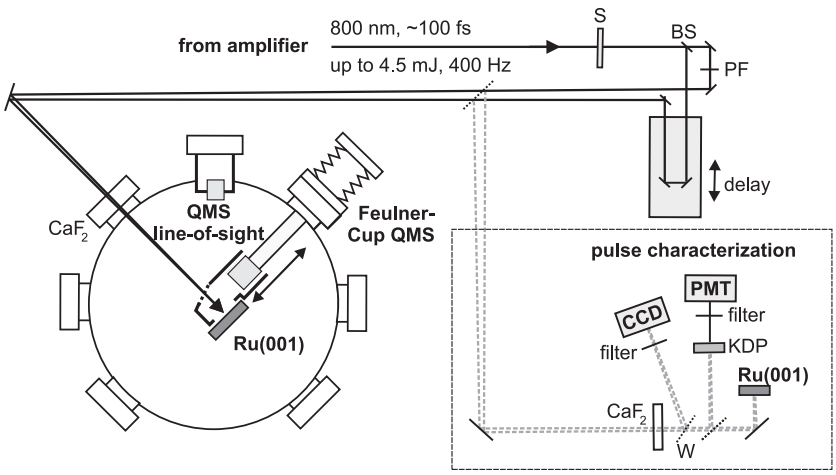

Figure 4. Experimental set-up for measurements of the fs-laser-induced desorption yield by mass spectrometry. Either a single pulse or a pulse sequence of two equally intense, cross-polarized fs pulses with variable time delay excite the adsorbate-covered surface of interest, here Ru(001). The reaction yield is measured either with a Feulner cup (see figure 5) or a line-of-sight quadrupole mass spectrometer. When the latter device is in operation as the detection unit, the Feulner-cup QMS is retracted and the Ru crystal rotated by 45° clockwise. In order to accurately determine the laser fluence relevant to the photoreaction, a precise pulse characterization is mandatory. In a reference beam channel (with optical components identical to those in the actual measurement beam path), the pulse profile is recorded with a gateable CCD camera at a position equivalent to the sample under UHV. A reference Ru crystal is employed to minimize the risk of beam damage at high fluences. A photomultiplier tube (PMT) is used for second harmonic autocorrelation traces. S, BS and PF stand for shutter, beamsplitter and polarization flipper, respectively.

from 30 to 1530 K. The chamber is equipped with two quadrupole mass spectrometers (QMSs), see figure 4, one of them attached to the bottom of the chamber allowing optical access through the cross beam ionizer. In the line of sight of this QMS, TOF spectra of molecules desorbed by a laser pulse can be recorded. The other QMS is mounted on a retractable translation stage aligned radially to the centre of the chamber (figure 4) and provides a much higher collection efficiency by a home-built glass enclosure around the ionization region (a so-called 'Feulner cup' [56]). With the sample set directly before an orifice in the enclosure, optical access is ensured through an optical-grade fused silica window clamped to the glass body on the opposite side to the Ru crystal (see photo in figure 5(a)). This way, desorbing molecules undergoing multiple collisions with the inner glass walls are guided towards the QMS ionizer, however, losing angular-distribution and flight-time information (figure 5(b)). Both QMSs can be used for TDS experiments, whereby spectra taken with the high-collection efficiency QMS exhibit a significantly enhanced signal-to-noise ratio by at least one order of magnitude as compared to the signal of the conventional QMS as illustrated by the H_2 TDS spectra of figure 5(c).

The general principle of an optical pump–mass spectrometry probe experiment is depicted in figure 4, where either a single pulse or a pulse sequence of two equally intense, cross-polarized (to avoid interference effects) amplifier pulses with variable time separation are sent onto the adsorbate-covered surface. Subsequently, on their way to the mass spectrometer, the desorbing product particles spread in time due to their reaction-specific translational energy distribution. In the case of hydrogen desorption from ruthenium, the formed H_2 (or D_2) molecules have such a high velocity (~5000 m s^{-1}) that for typically available flight distances of 15–20 cm the resulting arrival-time distribution remains very narrow, easily saturating the QMS device in the single-molecule counting mode. By contrast, the Feulner cup smears the nascent TOF spectra out in time over approximately two orders of magnitude (figure 5(d)). This makes the Feulner-cup QMS the device of choice in experiments where the overall reaction yield, i.e. the time *integral* of the arrival-time distribution, is wanted. Yet such a time integral as a single-shot entity is naturally subject to laser fluctuations. To overcome these uncertainties, the reaction yield is recorded for a series of laser pulses all impinging on the same spot on the sample. Since the adsorbate coverage is then gradually depleted during such multiple-pulse excitations, the declining yield may then be fitted to a reaction-kinetics-dependent decay curve. Thereby, fluctuations in the first-shot yield (FSY) are substantially reduced.

Figure 6 shows such decay curves for the fs-laser-induced H_2 association from an initially saturated Ru(001) surface (one monolayer (ML) H-(1 × 1)). While for lower fluences ($\langle F\rangle = 60$ J m^{-2}) approximately 20% of the initial desorption yield is still maintained even after 50 laser shots, the hydrogen coverage is almost entirely depleted at high fluences ($\langle F\rangle = 270$ J m^{-2}) within the first few laser shots. The solid lines in figure 6 are based on calculations according to the following: the number of desorbing molecules N_i is assumed to scale proportionally with the change in coverage $\Delta\theta_i$. For a bimolecular reaction, this in turn is proportional to the square of the initial coverage θ_i (before the ith laser pulse), i.e. $N_i \propto \Delta\theta_i = -\theta_i^2 f(F_i)$ with $f(F_i)$ being the functional relationship between yield and fluence [57]. Integration gives the decay of coverage with laser shot number j according to [16]

$$\theta_j = \frac{\theta_0}{\theta_0 \beta F_{\text{eff}}(j) + 1} \tag{9}$$

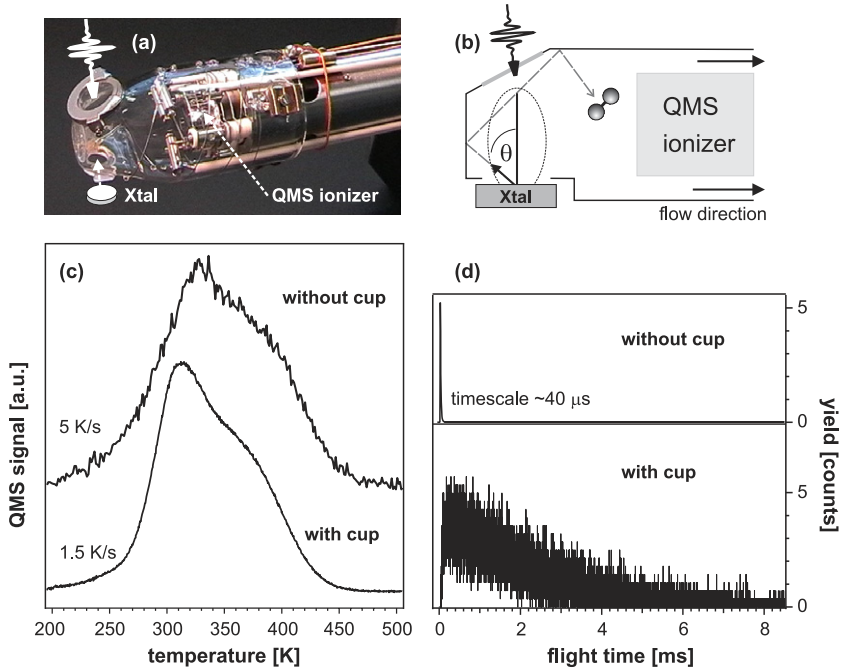

Figure 5. Solid-angle integrating quadrupole mass spectrometer device, resulting thermal desorption data and time-of-flight spectra in fs-laser-induced desorption experiments. (a) Photograph of the QMS whose high-collection efficiency is achieved through a glass enclosure (length 80 mm, diameter 33 mm) around the front part of the device. The desorbing reaction products are guided to the ionizer. Overlaid artwork indicates the incident femtosecond laser pulse entering the glass enclosure through a optical-grade quartz window. The adsorbate-covered crystal is set on the opposite side in front of an orifice in the cup. (b) Schematic sketch of the QMS device illustrating a potential pathway of a desorbing molecule which undergoes several inner wall collisions towards the ionization region. Thus, flight-time and angular-distribution information is lost. (c) Thermal desorption spectra of H_2 from Ru(001) taken with and without the Feulner cup, demonstrating the increased signal-to-noise ratio. Note the different heating rates. (d) Arrival-time distribution of H_2 after fs-laser excitation of an H-saturation coverage on Ru(001) with and without the cup. The time window, in which H_2 molecules reach the detector, is stretched from ∼40 μs to several ms. Parts of this figure adapted from [16].

where in the case of a nonlinear fluence dependence (as in the hydrogen recombination), $F_{\text{eff}}(j) = \sum_{i=1}^{j} F_i^n$ describes the effective, since accumulated, incident laser fluence [34, 57]. n is here a power-law exponent, as is usually done in a parametrization approach to the nonlinear fluence dependence of the reaction yield, (for details see below) and β a scaling constant with $f(F_i) = \beta F_i^n$. An effective cross section for the photoreaction may then be defined by the ratio of the decay-curve exponents of the *nonlinear* versus the *linear* fluence dependences, $\sigma_{\text{eff}} = \beta \sum F_i^n / \sum F_i$. This simplifies to $\sigma_{\text{eff}} = \beta F^{n-1}$ for pulses of identical fluence ($F_i = F =$ const).

As already mentioned, the yield of a fs-laser-induced surface reaction is usually nonlinearly dependent on the absorbed fluence of the exciting laser. As a consequence, for non-flattop beam profiles, beam sections of higher intensity contribute to the overall reaction yield to a higher extent than sections of lower beam intensity do (figure 7(b)). In order to compare yield data obtained with different spatial laser beam profiles, it is essential to account for the nonuniform energy distribution across the laser beam (figure 7(a)). This is realized by recording the experimental pulse energy and the spatial beam profile of the exciting laser for each measurement. A yield-weighing procedure [34, 50] is then applied in which each beam profile fraction of constant intensity is weighted with its respective yield resulting in the absorbed yield-weighted fluence $\langle F \rangle$. By parametrization of the fluence dependence of the desorption yield Y with a power law $Y \propto F^n$, $\langle F \rangle$ is obtained by summing over each camera pixel

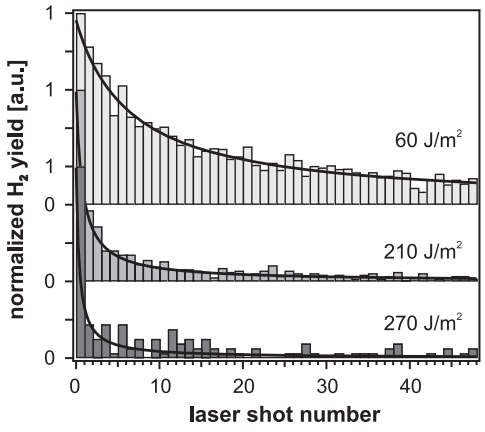

Figure 6. Femtosecond-laser-induced H_2 desorption yield from an H-saturated Ru(001) surface as a function of shot number within a series of 50 pulses impinging the same spot on the sample. This depletion of the coverage after multiple excitation can be used to derive an effective cross section for desorption (see text) which varies strongly with the absorbed fluence $\langle F \rangle$, here ranging from 60 to 270 J m^{-2}. Reprinted with permission from [16]. Copyright 2004 American Chemical Society.

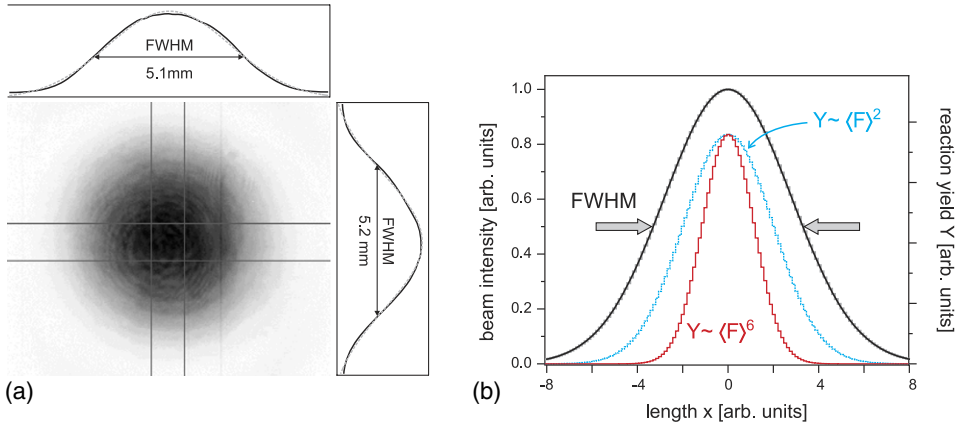

Figure 7. Non-flattop beam profile of the exciting laser pulse and the effect of a nonlinear fluence dependence of the reaction yield. (a) Spatial beam profile of a typical fs-laser pulse in the desorption experiments recorded with a CCD camera at a reference position equivalent to the actual sample under UHV conditions. The horizontal and vertical intensity distributions are averaged line cuts within the indicated ranges. Gaussian fits excellently reproduce the cuts with FWHMs of 5.1 and 5.2 mm, respectively. (b) An idealized Gaussian intensity distribution across the beam profile is assumed. As the yield of a fs-laser-induced surface reaction is usually nonlinearly dependent on the absorbed fluence (see figure 12), exemplary power laws with $Y \propto F^n$, $n = 2$ and 6, respectively, are plotted here normalized. This illustrates how beam sections of higher intensity contribute to the overall reaction yield to a much higher extent than sections of lower beam intensity do. To compensate for this effect, a weighting procedure is applied which weights the intensity of each camera pixel (like that of panel (a)) with its power-law-parametrized yield (see text).

according to

$$\langle F \rangle = \sum Y_i F_i \Big/ \sum Y_i = \sum F_i^{n+1} \Big/ \sum F_i^n, \qquad (10)$$

with n as a parameter of the self-consistent fit to the experimental dataset. Consequently, throughout this review, $\langle F \rangle$ is given as the absorbed yield-weighted fluence for full characterization of the laser-excitation condition.

3.2. State-resolved detection

While in the experiments described in the previous subsection with optical pump and subsequent mass detection of the desorbing product particles as the probe, the number of these molecules is recorded as a function of, for instance, the laser fluence, the time separation within a pulse sequence or the flight time from the surface to the mass detector, experiments in the current subsection with state-selective detection based on laser spectroscopic techniques address the *internal* degrees of freedom of the product molecules. To this end, the reaction initiating fs-laser system needs to be synchronized to a tunable detection laser fired a short time after desorption has occurred. The two commonly used detection methods, laser-induced fluorescence (LIF) and resonance-enhanced multiphoton ionization (REMPI), both excite the desorbing species resonantly to an electronic state. The excited molecules then either relax radiatively with a initial quantum-state-dependent fluorescence signal (LIF), or they are photoionized by one or more additional photons (REMPI) and subsequently detected by an ion detector [3]. In both techniques, molecules only in a specific quantum state are detected when the probe laser is tuned to a particular transition between quantum states with certain electronic, vibrational and rotational quantum numbers.

In the case of the hydrogen association from ruthenium, the REMPI technique has been employed in state-selective measurements of the desorbing D_2 molecules induced by fs-laser excitation [58]. While the same fs-laser system as in section 3.1 was used, a narrow-bandwidth nanosecond vacuum ultraviolet (VUV) laser source was set up and synchronized to the fs system at 10 Hz. The detection laser system (see figure 8) is based on a Nd:YAG laser-pumped dye laser whose second harmonic is then frequency tripled in a krypton cell [59] yielding tunable VUV laser radiation in the $\lambda = 106$–110 nm spectral range. This radiation serves as the resonant excitation step in a $(1 + 1')$ REMPI process. For normalization reasons, the VUV intensity is recorded for each single laser pulse via the ion signal produced in an acetone-filled monitor cell, which is attached to the exit window of the UHV chamber. In addition, an unused portion of the fundamental output of an Nd:YAG laser is quadrupled which yields UV photons at $\lambda = 266$ nm and is used for the non-resonant step in the multiphoton ionization of the excited D_2 species.

To obtain a sufficient signal-to-noise ratio in the ion signal during the pulsed experiment, a steady state of the surface coverage is aimed for, since in femtochemistry studies on surfaces the sample under investigation is not as easily refreshed as in molecular beam arrangements of gas phase experiments. One option to avoid otherwise time-consuming preparation/laser-excitation cycles is to redose the adsorbed reactants via the background pressure. However, for the H/Ru system, molecular redosing has to be ruled out, since offered hydrogen molecules by this means are indistinguishable from desorbing species of the photoinduced reaction, and moreover, atomic hydrogen dosing often suffers from unsatisfactory particle purity. For this reason, without redosing, the focused beam of the fs laser has to be scanned over the deuterium-covered ruthenium surface by moving the crystal via computer-controlled stepper motors. In order to detect the desorbing

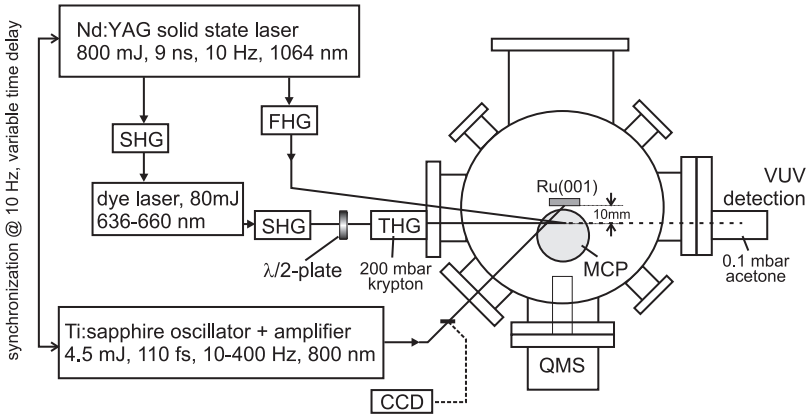

Figure 8. Experimental set-up for state-selective measurements of the desorbing product particles based on REMPI spectroscopy. The reaction initiating amplified femtosecond laser is synchronized with a tunable detection laser system (here, a VUV source based on a solid-state-laser-pumped dye laser, which is frequency doubled (SHG) and subsequently tripled (THG) in a rare gas cell (krypton)). The desorbing molecules are ionized at a position close to the sample surface (here, Ru(001)) via a resonant VUV excitation together with a non-resonant UV transition. An MCP ion detector mounted underneath the Ru crystal records the ionized species as a function of the VUV wavelength. The polarization of this resonant radiation might be rotated with a half-wave plate between the SHG and THG stages. For normalization of the ion signal with respect to the VUV intensity, an acetone-filled monitor cell is used. (SHG, THG and FHG indicate second, third, and forth harmonic generation, respectively. MCP stands for microchannel plate.) Reprinted with permission from [58]. Copyright 2005 American Physical Society.

D_2 molecules, the UV and VUV laser beams are brought into spatial overlap under a small angle in a plane parallel to the crystal surface at a certain distance in front of the Ru crystal (see figure 8). The temporal delay between the fs and the VUV laser is adjusted such that only molecules at the maximum of the TOF spectrum are ionized. This guarantees that a molecular sub-ensemble of almost identical velocity is probed. The deuterium molecules are electronically excited by the VUV radiation to the $B\ ^1\Sigma_u^+(v', J') \leftarrow X\ ^1\Sigma_g^+(v'', J'')$ Lyman band system. In a second step, the UV photons ionize the excited D_2 molecules which are eventually detected by microchannel plates (MCP) mounted underneath the Ru crystal in a lower plane of the UHV chamber. In addition, and only accessible in a $(1 + x)$ REMPI scheme, the rotational quadrupole alignment $A_0^{(2)}$ of the desorbing molecules, here D_2, can be determined by changing the polarization of the excitation photons via a half-wave plate before the tripling unit [58, 59].

3.3. Vibrational spectroscopy

All-optical pump–probe measurements offer the possibility to trace a surface reaction in real time, whereby the reaction is triggered by an ultrashort pump pulse, and the reactants' response is monitored by a molecule-specific and surface-sensitive probe such as vibrationally resonant sum-frequency generation (SFG). Figure 9 shows a typical experimental set-up for time-resolved SFG studies with details on how the broadband vibrational spectrum of the sample is obtained [34, 60]: a femtosecond IR pulse generated in a optical parametric amplifier with subsequent difference frequency mixing induces a polarization in the adsorbate within a spectral window of $\sim$150 cm^{-1}. A picosecond, i.e. spectrally narrow (since truncated in a pulse shaper), VIS pulse up-converts this IR polarization into broadband SFG light which is then dispersed and detected by a spectrometer/CCD camera set-up. The SFG signal is resonantly enhanced, if the incident IR frequencies match a molecular vibrational mode of the adsorbate; thus one probes the chemical identity and local bonding in the adsorbate layer. In time-resolved experiments, the pair of IR/VIS pulses are preceded by an intense pump pulse which initiates the dynamics of the surface process. Prominent examples for such SFG studies in surface femtochemistry are the CO desorption from ruthenium (Ru(001)) [61] and the CO diffusion from step to terrace sites on platinum (Pt(533)) [12].

Although the SFG spectroscopy technique described so far has not been explicitly applied to the H/Ru(001) system, a different type of experiment aiming towards control of a surface reaction, in particular the vibrational enhancement of hydrogen desorption from Ru(001), is related to the way of IR frequency generation as depicted in figure 9. The principal approach is to pre-excite the adsorbate system vibrationally in the IR in such a way that a second reaction-initiating laser pulse leads to an enhanced desorption yield, if the vibrational excitation remains localized long enough. As will be detailed further in section 5, theory predicts a desorption increase of about one order of magnitude, depending on the addressed vibrational mode (H–H interatomic stretch versus H_2–surface distance vibration at 13.2 and 9.1 μm, respectively) [62, 63]. The generation of such laser frequencies in the mid- to (almost) far-IR spectral range is basically feasible with the TOPAS as the IR source; sufficient pulse energies, however, remain a challenge.

4. Hydrogen association from Ru(001)

Hydrogen recombination on ruthenium, $H_{ad} + H_{ad} \rightarrow H_{2,gas}$ on Ru(001), may be initiated thermally (i.e. under conditions of thermal equilibrium between all degrees of freedom),

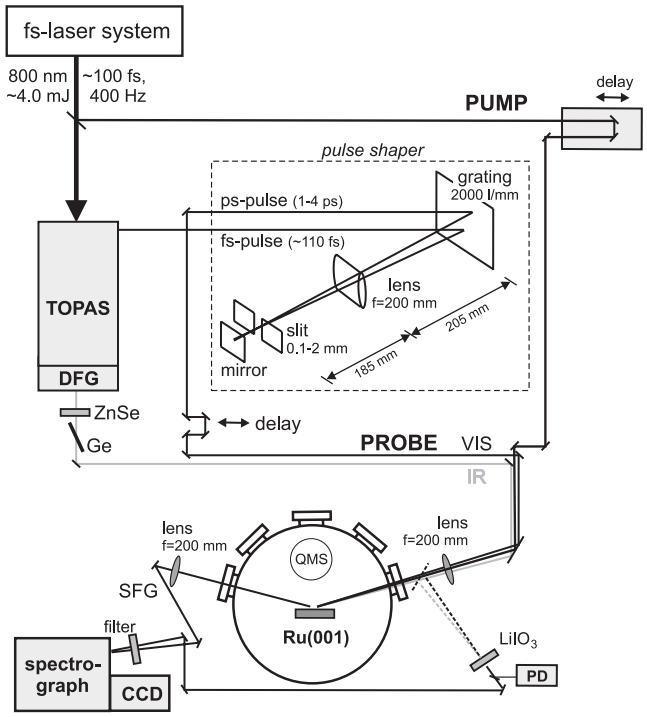

Figure 9. Detailed optical layout for vibrational sum-frequency generation (SFG) experiments with molecular adsorbates on surfaces. Mid-IR frequencies resonant with intramolecular vibrational modes are obtained by a (travelling-wave) optical parametric amplifier (of superfluorescence), TOPAS, and subsequent difference frequency generation (DFG) between signal and idler in a further nonlinear crystal ($AgGaS_2$). In broadband SFG with ultrashort laser pulses, the VIS (800 nm) up-conversion pulse is obtained using the residual pump of the TOPAS which is spectrally truncated, hence a few ps long and about 5 cm^{-1} wide. Both fs IR and ps VIS pulses irradiate the adsorbate-covered sample in the UHV chamber under grazing incidence. The generated SFG light leaves the chamber accordingly, is then spectrally filtered and dispersed in a grating spectrometer. The broadband SFG spectrum is recorded with an intensified CCD camera. To monitor spatial and temporal overlap of the IR and VIS radiation, a nonlinear $LiIO_3$ crystal is employed which is placed outside the chamber at a position equivalent to the sample under UHV. In time-resolved SFG experiments, the sample is first excited by a strong pump pulse and subsequently probed at variable delays by the pair of IR/VIS pulses.

but if induced by fs-laser excitation several characteristic differences are observed: (i) there is a large isotope effect between H and D, i.e. H_2 is much more readily formed than D_2. Such a difference is absent in the thermally initiated reaction. (ii) Desorption of the heavier isotope (D_2) is facilitated, i.e. promoted by the presence of the lighter counterpart (H_{ads}) on the surface. Furthermore, a peculiar threshold-like coverage dependence is found in the laser-induced reaction apparently contradicting statistical nearest-neighbour arguments. (iii) The H_2 (and D_2) molecules coming off the surface exhibit appreciable kinetic excess energy with corresponding translational temperatures much higher than one would expect from thermal desorption spectroscopy. Apparently, the hydrogen molecules induced by fs-laser pulses leave the surface excited without complete equilibration with the heat bath of the solid. Details of all these observations will now be discussed in the following subsections.

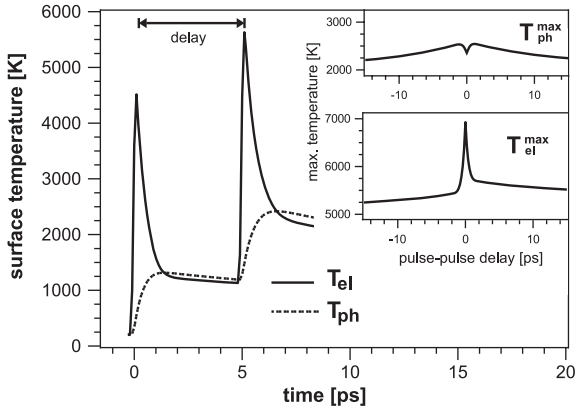

Figure 10. Two-temperature model calculations of the electron and phonon temperature transients $T_{el}(t)$ and $T_{ph}(t)$ at the surface of an Ru sample after excitation with a pair of two ultrashort laser pulses separated by 5 ps (800 nm, 110 fs, $2 \times \sim 120$ J m^{-2}). The inset shows the maximal temperatures T_{el}^{max} and T_{ph}^{max} as a function of the pulse–pulse delay which illustrates that a two-pulse correlation trace of an electron-mediated process is much narrower in time than the corresponding correlation of phonon-mediated energy transfer. The dip in T_{ph}^{max} at zero time delay is caused by the competition between electron–phonon coupling and hot-electron heat transfer away from the surface [39]. The apparent asymmetry in the T_{el}^{max} trace originates from small (usually experimentally inevitable) deviations from perfectly equal beam intensities of the two pulses. Figure adapted from [34].

4.1. Excitation mechanism of fs-laser-driven reaction

As outlined in section 2.2 and illustrated by figures 1 and 3, in a substrate-mediated surface reaction, each of the substrate's subsystems, electrons and phonons, can couple to the reactants in the adsorbate layer independently. The appropriate experimental approach to unambiguously distinguish a phonon- from an electron-mediated reaction mechanism is to measure the two-pulse correlation (2PC) of the reaction yield [6]. In such an experiment, two equally intense fs-laser pulses excite the sample with a variable time delay Δt between them. The reaction yield is then detected as a function of Δt. Due to the typical nonlinear dependence of the reaction rate on the incident laser fluence (see further below, figure 12(a)), the width of the resulting yield correlation function critically depends on the excitation pathway. A narrow full width at half-maximum (FWHM) of only a few picoseconds is a clear indication for the operation of a hot electron, i.e. DIMET-like reaction mechanism, since only for pulse separations shorter than the electron–phonon equilibration time is the electron temperature greatly enhanced due to the combined effect of both excitation pulses. In contrast, a phonon-mediated process proceeds on a much slower timescale of tens of ps due to the significantly longer energy storage time within the phonons compared to that of the electronic system and the slower coupling time from the phonon bath into the reaction coordinate.

How the excitation by a two-pulse sequence leads to the described features of the yield correlation function can be rationalized with the aid of figure 10. Calculated with the 2TM (equations (1) and (2)) for an exemplary pulse–pulse

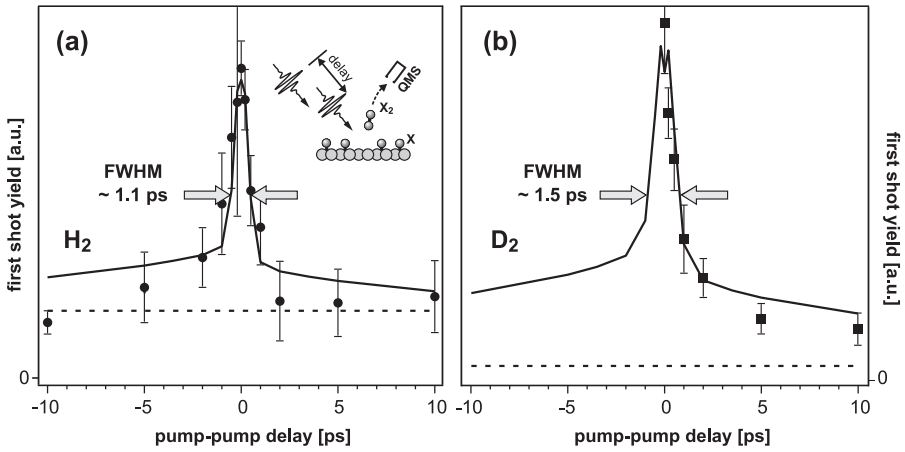

Figure 11. Two-pulse correlation of the fs-laser-induced desorption yield of hydrogen H_2, panel (a), and D_2, panel (b), from Ru(001). The yield of the first shot out of a series of laser pulses (see figure 6) is plotted as a function of delay between the almost equally intense pulses (intensity ratio 54:46). The narrow correlation width of both datasets ($FWHM_{H_2} = 1.1$ ps, $FWHM_{D_2} = 1.5$ ps) indicates a hot-substrate electron-mediated energy transfer mechanism to be operative. The solid lines mark the outcome of the theoretical modelling (two-temperature model with subsequent electronic friction, see text). Part of the figure adapted from [16].

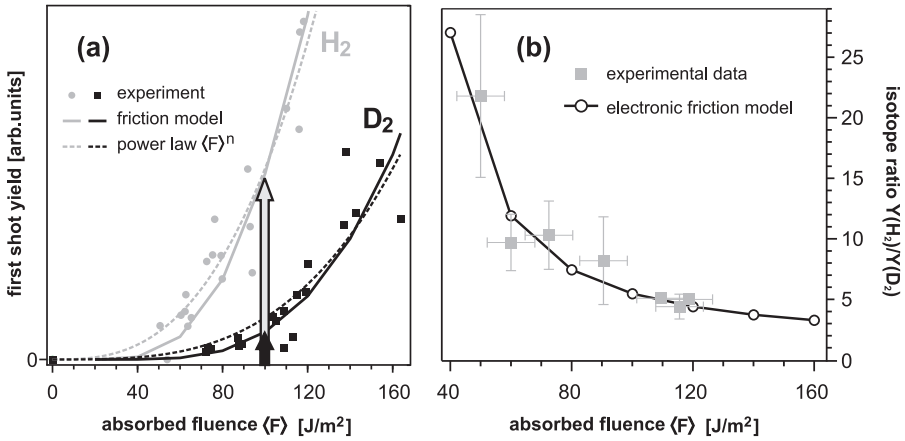

Figure 12. Femtosecond-laser-induced hydrogen desorption from a saturated Ru(001) surface. (a) Fluence dependence of the H_2 and D_2 yield together with friction model calculations and power-law parametrizations $Y \propto \langle F \rangle^n$ with $n = 2.8$ and 3.2 for H_2 and D_2, respectively. Arrows indicate the observed isotope effect for an exemplary fluence of $\langle F \rangle = 100$ J m^{-2}. (b) Fluence dependence of the isotope yield ratio between H_2 and D_2 (experimental data points and friction calculations). Figure adapted from [16].

delay of $\Delta t = 5$ ps, the ruthenium surface is excited by two fs pulses, leading to an electronic and phononic temperature–time profile similar to that of figure 1(c), however, with the second pulse striking the surface while both subsystems are still at elevated temperatures. If one now plots the maximum temperature T_{el}^{max} and T_{ph}^{max} reached in the electron and the phonon heat bath as a function of Δt, a narrow and a broad maximum temperature distribution is obtained, respectively. For $T_{el}^{max}(\Delta t)$, this can be understood by the sharp rise and fall of the electronic temperature transient $T_{el}(t)$ while the phonon temperature cools significantly more slowly. Consequently, due to the nonlinear relation between T_{el} and T_{ph}, respectively, and the adsorbate temperature T_{ads} (see the Arrhenius-type factor in equations (6) and (8), respectively), the two-pulse correlation of the reaction rate R, and hence the yield as the time integral of R, reflects the respective width of these peak temperature distributions. It is noteworthy that the electron–phonon equilibration time is comparatively short for Ru of ~1 ps, causing this temporally narrow electronic temperature transient as seen in figure 10. Metals like Cu or Au in contrast exhibit a significantly weaker electron–phonon coupling with coupling constants g by one to two orders of magnitude smaller [39], which in turn smears out the respective electronic and phononic temperature transients.

Figure 11 displays the outcome of such 2PC measurements for the associative H_2 (D_2) desorption from Ru(001). A narrow yield correlation is observed with a FWHM of ~1 ps indicating an energy transfer pathway predominantly driven by hot-substrate *electrons* [16, 19]. Furthermore, the fluence dependence of the desorption yield for both isotopes H_2 and D_2 from a respective H or D layer on Ru(001) is depicted in figure 12(a). The clear nonlinear relationship reflects that, in accordance with a DIMET process, multiple excitation/deexcitation cycles occur until desorption is completed [6, 10, 17]. In addition, this nonlinearity underlines how essential it is to account for an energetically nonuniform spa-

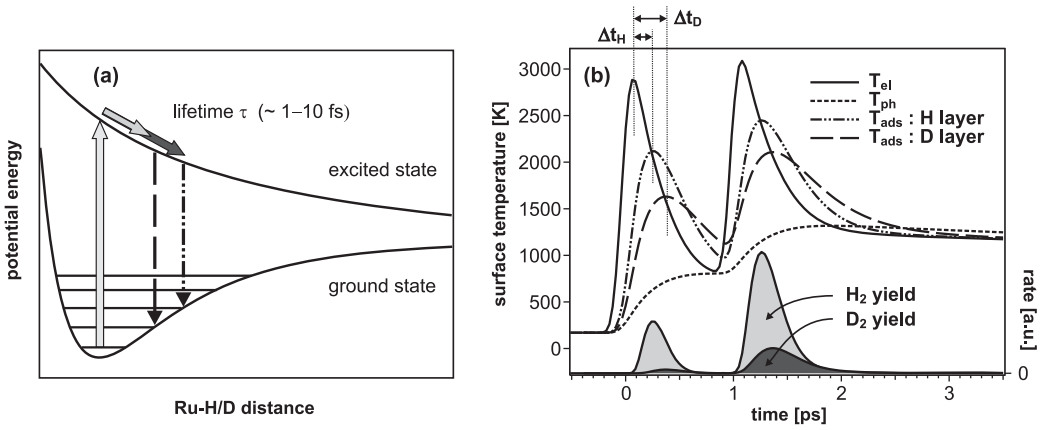

Figure 13. Rationalizing the isotope effect in fs-laser-induced desorption reactions. (a) In the DIMET picture, due to the chemical identity, both isotopes are transferred to the same excited PES. However, the lighter reactants travel a larger distance on the excited surface during the short lifetime of a few fs and consequently gain more vibrational energy after relaxation back to the ground PES than the heavier counterparts do. (b) In the friction picture, due to the stronger adsorbate–substrate coupling (i.e. shorter energy coupling times) of the lighter reactants, here H with respect to D, an H adlayer heats up earlier and reaches higher temperatures than a respective D adlayer. This is quantified by the time differences Δt_H and Δt_D between the peak electronic temperature and the maximum in the corresponding adsorbate temperature $T_{ads}(H)$ versus $T_{ads}(D)$. Calculations based on the two-temperature model in conjunction with the electronic friction model are performed here for two 130 fs pulses of 60 J m^{-2} each with a pulse–pulse separation of 1 ps. Panel (b) reprinted with permission from [19]. Copyright 2003 American Physical Society.

tial beam profile of the exciting laser with a yield-weighting procedure [16, 34, 50] as detailed in section 3.1 and illustrated by figure 7.

Further corroboration for a reaction mechanism driven by hot-substrate electrons is found when one compares absolute desorption yields per laser shot from H/Ru(001) and D/Ru(001), respectively. It is significantly easier to form the lighter isotope H_2 by fs-laser excitation than the heavier D_2 molecules. In addition, this isotope yield ratio $Y(H_2):Y(D_2)$ exhibits a remarkable fluence dependence as plotted in figure 12(b). The exceedingly high values for $Y(H_2):Y(D_2)$, at low fluences even larger than 20, reflect the extraordinary mass ratio of the reactants of 2:1. A clear isotope effect is a general phenomenon for an electron-driven reaction mechanism. In contrast, phonon-mediated processes typically exhibit—if at all—only very small isotope effects [64], consistent with the absence of any differences between H_2 and D_2 TD spectra from Ru(001) [19]. The solid lines in figures 11 and 12 represent the outcome of theoretically modelling the data using the two-temperature model [9, 33] together with the modified electronic friction model [18, 45]. All experimental findings (2PC data, yield fluence dependences and isotope effect) can be well reproduced within the framework of these models with a single parameter set consisting of an activation energy E_a of 1.35 eV and energy coupling times of 180 and 360 fs for H_2 and D_2, respectively. Note that τ_{el} for D_2 is scaled in accordance to Brandbyge *et al*'s mass proportionality $\tau_{el} \propto m$ [45], which provides a very good fit to the D_2 data.

The origin of the isotope effect in the yield of surface femtochemistry reactions is typically rationalized in the DIMET picture, in which the lighter reactant will have gained more vibrational energy after relaxation back to the ground state than its heavier counterpart due to the mass-dependent acceleration on the excited PES (see figure 13(a)). Likewise the difference in the fs-laser-induced desorption yield between H_2 and D_2 can be explained from the perspective of the frictional description of a femtochemical reaction (figure 13(b)). Due to the electronic nature of the excitation mechanism (i.e. the different coupling times for H and D, respectively), the adsorbate temperature T_{ads} of both layers (H and D) follow the electronic temperature T_{el} with a certain delay Δt_X, X = H; D. However, the faster coupling time for an H layer causes the transient adsorbate temperature T_{ads}(H) of an H layer to rise earlier and reach higher values as compared to T_{ads}(D) for a D layer. The slower coupling time for the heavier D atoms is responsible for the fact that the electronic temperature T_{el} has already passed its maximum when the D layer starts being excited. As a consequence of the nonlinear dependence of the reaction rate on the adsorbate temperature, the difference in the desorption yields between both isotope is even enhanced, resulting in pronounced isotope effects. This applies in particular to the H_2 versus D_2 recombination reaction with the largest mass ratio possible.

4.2. Adsorbate–adsorbate interactions

In general, reactants adsorbed on a solid surface interact with their surroundings, both with other neighbouring reactants, which eventually leads to the chemical reaction, and with those adsorbates which do not directly participate in the chemical reaction but modify the electronic structure of the adsorbate–substrate complex. For the H(D)/Ru(001) system, experiments with isotopically mixed hydrogen adlayers reveal an intriguing consequence of adsorbate–adsorbate interactions operative in the recombination process [19]. Starting with a saturation coverage, but with varying proportions of both isotopes H and D, the total yield of all three product molecules H_2, D_2 and HD is measured for both excitation methods, thermal activation and excitation with fs-laser pulses. Under thermal equilibrium conditions, typical TD spectra are obtained whose

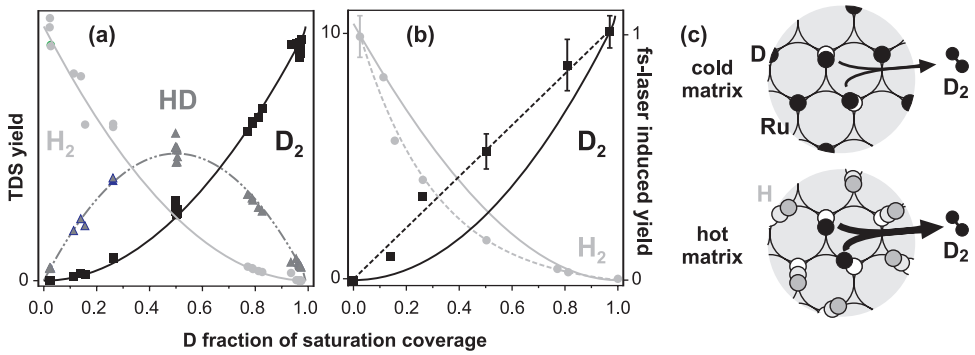

Figure 14. Hydrogen desorption from a saturation coverage H/D[1 × 1] on Ru(001) with varying proportions of H and D. Mixtures are characterized by the D fraction whereby 0 corresponds to a pure H layer while 1 marks the pure D layer. (a) Thermally induced yields for all three isotopes H_2, D_2 and HD, respectively, as a function of the D fraction. Data points follow second-order reaction kinetics (solid lines) (b) Femtosecond-laser-induced recombination yields. Solid lines again describe the outcome of second-order rate equations, here, however, based on the time-dependent rate constants obtained with the friction model. Dashed lines are guides to the eyes. Note that more D_2 and less H_2 are formed in the experiment than theoretically expected, which is attributed to dynamic promotion effects. (c) Illustration of the dynamic promotion; the more rapid excitation of H atoms creates a hot matrix, in which the recombination producing D_2 molecules is enhanced as compared to surroundings where the D reactants are embedded in a relatively cold matrix of D atoms. Reprinted with permission from [19]. Copyright 2003 American Physical Society.

integrated yield is plotted in figure 14(a) as a function of the D concentration in these mixed layers, i.e. the D fraction of the total coverage. According to second-order kinetics, the rate equations

$$\frac{\mathrm{d}}{\mathrm{d}t}[\mathrm{H}_2] = k[\mathrm{H}]^2, \qquad \frac{\mathrm{d}}{\mathrm{d}t}[\mathrm{D}_2] = k[\mathrm{D}]^2, \qquad \text{and} \qquad \frac{\mathrm{d}}{\mathrm{d}t}[\mathrm{HD}] = 2k[\mathrm{HD}] \tag{11}$$

describe the change of each hydrogen isotope with time. While observing the mass continuities for H and D, i.e. $\mathrm{d}/\mathrm{d}t[\mathrm{H}] = -2\mathrm{d}/\mathrm{d}t[\mathrm{H}_2] - \mathrm{d}/\mathrm{d}t[\mathrm{HD}]$ and $\mathrm{d}/\mathrm{d}t[\mathrm{D}] = -2\mathrm{d}/\mathrm{d}t[\mathrm{D}_2] - \mathrm{d}/\mathrm{d}t[\mathrm{HD}]$ [19], respectively, numerical integration of equation (11) yields excellent agreement with the experimental data of the thermally induced hydrogen formation (solid lines in figure 14(a)).

In strong contrast, analogous experiments performed under fs-laser excitation indicate a much more complicated recombination process than a simple bimolecular reaction. Figure 14(b) shows the respective results of the fs-laser-induced desorption yields as a function of the D fraction. The yield ratio from pure adlayers, i.e. D fraction equals 0 and 1, respectively, amounts to 10:1 consistent with the isotope effect at a fluence of $\langle F \rangle = 60\ \mathrm{J\,m^{-2}}$ (see figure 12(b)). However, if one compares these experimental data with results of a rate equation modelling based on equation (11) now with time-dependent rate constants $k[T_{\mathrm{ads}}(t)]$ (see equation (8)), clear differences are observed. Significantly more D_2 is formed than predicted by the rate equation modelling. The presence of neighbouring H_{ads} species on the Ru surface obviously enhances the associative desorption probability of D_2 molecules[2]. In other words, a concerted action of more partners than only both reactants forming the respective hydrogen molecule seems to be involved. Such effects due to coadsorption of other species are known in heterogeneous catalysis as reaction promotion or poisoning (as the opposite effect) and originate from the coadsorption-induced changes in the electronic structure of the reaction system [65]. In the case of the fs-laser-induced hydrogen association from ruthenium, the D_2 yield enhancement is attributed to the faster energy transfer from the Ru substrate to an *H* adsorbate than to the heavier *D* (see above $\tau_{\mathrm{el}}(\mathrm{H}_2) = 1/2\,\tau_{\mathrm{el}}(\mathrm{D}_2)$). Hence, a surrounding consisting of H starts earlier exploring locations on the surface which favour the recombination of neighbouring D reactants than a D matrix, which is still relatively cold due to slower excitation as illustrated in figure 14(c). A physical picture of this *dynamic* promotion effect would involve attractive and/or repulsive interactions between the faster excited H atoms and the two D reactants. For small adsorbates like hydrogen, however, steric repulsion between neighbouring sites can be neglected and indirect, i.e. substrate-mediated, interactions dominate [66, 67]. Electronic changes in the adsorbate–substrate complex, e.g. changes in the reaction barrier and/or energetic shifts in the excited PES, might contribute. Consequently, in such a dynamic promotion process, the transient influence of the reactants' surrounding may reduce the activation energy for the desorption reaction and hence increase the rate constant [68]. In an even more general way, a bimolecular surface reaction/desorption can be reformulated as $A_{\mathrm{ads}} + B_{\mathrm{ads}} \xrightarrow{k[U(t)]} \mathrm{AB}$ with $U(t)$ describing the time-dependent surroundings. In moments of certain adsorbate–substrate conditions causing a reduced barrier height, altered excited state conditions and/or attractive/repulsive adsorbate–adsorbate interactions, a favourable energy landscape is created which leads to reaction. This microscopic picture also complies with thermally initiated surface reactions, in which statistical fluctuations cause the respective surroundings conditions.

[2] Note that, despite the apparent reduction of the H_2 yield in the presence of a D surrounding (figure 14(b)), the given explanation for yield enhancement still applies also for the H_2 recombination; without the promotion effect also for H atoms in an H surrounding, the isotope ratio between pure H and D coverages would have been smaller than the measured value of 10:1.

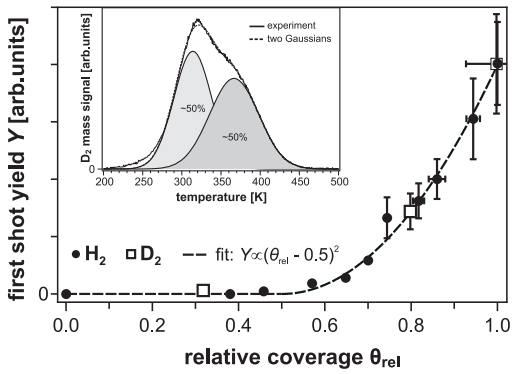

Figure 15. Coverage dependence of the fs-laser-induced hydrogen recombination from Ru(001) at an absorbed fluence $\langle F \rangle$ of 60 J m^{-2}. Apparently, both H_2 and D_2 obey the same Y versus θ_{rel} relationship. Adsorbate interactions are believed to cause a nearly threshold-like behaviour with yields detectable only above $\theta_{rel} = 0.5$. The quadratic dependence of the yield on coverage for $\theta_{rel} \geqslant 0.5$ is empirical (dashed line). The thermal desorption spectrum for D_2/Ru(001) shown in the inset exhibits two components with a second maximum only above $\theta_{rel} \approx 0.5$. This corroborates significant adsorbate interactions leading to differences in activation energies for desorption. Figure adapted with permission from [16]. Copyright 2004 American Chemical Society.

How adsorbate–adsorbate interactions further manifest themselves in the hydrogen/Ru(001) system is shown in figure 15, where a peculiar coverage dependence of the desorption yield from isotopically pure H or D layers is shown. Only for coverages θ above a threshold of ∼0.5 ML does the desorption yield rise above the detection limit and reach its maximum at the saturation coverage of $\theta = 1$ ML. Possible origins are the coverage dependence of the binding energy and/or of the electronic friction coefficient, but also the influence of the significantly lower barrier for diffusion at low coverage has been discussed recently [69]. The latter might prevent successful recombination events even at coverages with nearest neighbours. For instance, at $\theta = 0.5$ ML, each H_{ads} atom is still surrounded on average by two further adsorbed species such that association of two reactants should be statistically possible. Why, however, the coverage threshold seen in the fs-laser-induced recombination occurs at that particular value of $\theta = 0.5$ ML cannot be explained by diffusion, but is consistent with the following observation in thermally induced recombination. There as well, interesting evidence is found for distinct adsorbate–adsorbate interactions in the hydrogen/ruthenium system. The TD spectrum of 1 ML D_2 from Ru(001) (see inset of figure 15 and for H_2, figure 5(c)) exhibits a twofold feature, a characteristic maximum at 320 K and a shoulder around 380 K [19, 70]. Unlike the initial interpretation of the TDS data according to which the two desorption peaks originate from adsorbates on two different adsorption sites [70], it is now commonly accepted that hydrogen atoms on Ru occupy the threefold coordinated sites at all coverages [71] and that the shape of a hydrogen TD spectrum is caused by increasing adsorbate–adsorbate interaction at higher coverages. As also demonstrated in the inset of figure 15, two Gaussians of approximately equal integrated area give a good fit to the overall TD spectrum. Apparently, for both the thermally and the fs-laser-initiated recombination reaction, lateral interactions within the adsorbate layer become important for coverages $\theta > 0.5$ ML. Generally, coverage-dependent surface chemistry can originate from direct attractive, respectively repulsive, adsorbate–adsorbate interactions and/or coverage-dependent changes in the electronic structure of the adsorbate–substrate complex, similar to the dynamic promotion effect described afore. Even at low coverages, pronounced changes in the band structure of a metal substrate are observed, for example, in H-coverage-dependent photoemission experiments from Ni and Pd [72]. Such changes in the electronic structure may also affect the electronic friction coefficient and hence the coupling time τ_{el} for energy flow into the adsorbate coordinate. Therefore, both a coverage-dependent friction coefficient and changes in the adsorbate binding energy may contribute to the reported coverage dependence of the fs-laser-induced hydrogen desorption yield from Ru. Finally, additional corroboration of the importance of adsorbate–adsorbate interactions in hydrogen adsorption systems is found in scanning tunnelling microscopy (STM) studies by Mitsui *et al* [73] on the dissociative adsorption of hydrogen on Pd(111), the time reversal of an associative desorption process. The authors find that for a successful adsorption event on the Pd surface not only both reactants (i.e. the two H atoms) but also the surroundings play a crucial role. The adsorbing H_2 molecule seems to require, contrary to conventional thinking, more than the necessary two-vacancy sites (i.e. three or more contiguous vacancies) on the Pd surface for an effective adsorption reaction.

4.3. Energy partitioning

Investigations on the energy partitioning between different (translational, vibrational, rotational) degrees of freedom of the reaction product in a surface reaction offer additional insights into the underlying excitation mechanism and the pathway of energy flow. Under reaction conditions close to thermal equilibrium, e.g. in thermal desorption or with ns-laser pulse excitation, non-activated reaction systems typically show an equally balanced energy partitioning, while the reaction proceeds adiabatically on the electronic ground state. In contrast, activated systems usually exhibit an energy content of the reaction product which is unequally distributed between the different degrees of freedom. Depending on the location of a reaction barrier in the entry or exit (with respect to *ad*sorption) channel of the electronic ground state, translational or vibrational excitation may facilitate the reactants to overcome the transition state [74], hence the terms ‘translational’ and ‘vibrational’ barrier, respectively. The topology of the PES also determines to which extent in a recombinative desorption reaction the initial excitation normal to the surface at an early stage of the reaction might be converted to lateral and ultimately to interatomic motion, i.e. vibration. Nonadiabatic effects, however, can also result in an unequal energy transfer into different degrees of freedom of the reaction product as seen, for instance, in the ns-laser experiments on the associative desorption of N_2 from Ru(001)

by Diekhöner *et al* [75]. In these studies, contrary to expectations for a vibrational barrier, the nascent N_2 molecules carry only little vibrational energy. Apparently, they lose most of their energy on their way beyond the reaction barrier which was explained by strong nonadiabatic coupling of the vibrational coordinate to electron–hole pairs.

Rather high translational energies are obtained from TOF measurements of the desorbing product molecules in the fs-laser-induced associative H_2 and D_2 desorption from Ru(001) [58], an observation which indicates on its own that a reaction mechanism is operative in the ultrafast-laser-driven reaction different from that in the thermally initiated process. Mean translational energies (and respective translational temperatures) are derived much higher than one would expect from thermal desorption spectroscopy with no significant translational barrier assumed. These high translational temperatures, at least, point to hydrogen molecules departing from the Ru surface after fs-laser excitation without complete equilibration with the metal substrate. For D_2, translational temperatures $T_{\mathrm{trans}} = \langle E_{\mathrm{trans}}\rangle/2k_{\mathrm{B}}$ extracted from the second moment of the experimental TOF distributions range from ~2000 K at a relatively low absorbed fluence $\langle F\rangle$ of 50 J m^{-2} to over 3200 K at $\langle F\rangle = 140$ J m^{-2}, demonstrating a pronounced fluence dependence (see figure 16(a)). The lighter H_2 (data not shown here) even reaches temperatures T_{trans} of more than 4000 K at the highest fluence applied (140 J m^{-2}), underlining a clear kinetic isotope effect [58]. Both the trend of increasing $\langle E_{\mathrm{trans}}\rangle/2k_{\mathrm{B}}$ with increasing $\langle F\rangle$ and the isotope effect in the translational energies between D_2 and H_2 are qualitatively reproduced by friction calculations whereby an averaged adsorbate temperature $T_{\mathrm{ads}}^{\mathrm{RW}}$ is used. $T_{\mathrm{ads}}^{\mathrm{RW}}$ is defined as $T_{\mathrm{ads}}^{\mathrm{RW}} = \int_0^\infty T_{\mathrm{ads}} R(t)\,\mathrm{d}t / (\int_0^\infty R(t)\,\mathrm{d}t)$ with T_{ads} and $R(t)$ as the adsorbate temperature and rate, respectively, obtained from the friction model [18, 45], and it may be rationalized that this temperature describes the energy content relevant to the reaction in a more representative way due to the weighting procedure than just the mere maximum of the temperature transient $T_{\mathrm{ads}}(t)$ [58].

Information on the energy content transferred to internal degrees of freedom during the formation reaction of D_2 is gained through state-resolved detection of the desorbing molecules in a $(1+1')$ REMPI process using $B\,^1\Sigma_u^+(v', J') \leftarrow X\,^1\Sigma_g^+(v'', J'')$ Lyman bands of the D_2 species as resonant transitions [58], see section 3.2. Figure 16(b) displays Boltzmann plots (i.e. semi-logarithmic representations of the normalized populations $N(v, J)$ as a function of rotational energy) for the vibrational ground and first excited state revealing a non-thermal rotational population distribution. In particular, low J states in the ground vibrational state $v = 0$ seem to be overpopulated. However, one can still calculate the respective mean rotational energy in the $v = 0$ state yielding $\langle E_{\mathrm{rot}}^{v=0}\rangle/k_{\mathrm{B}} = 800$ K. In contrast, in the first vibrationally excited state, the rotational population obeys a Boltzmann distribution and hence can be assigned formally to a rotational temperature of $T_{\mathrm{rot}} = \langle E_{\mathrm{rot}}^{v=1}\rangle/k_{\mathrm{B}} = 1500$ K. Weighting with the population of the corresponding quantum states, a common rotational temperature $T_{\mathrm{rot}} = E_{\mathrm{rot}}/k_{\mathrm{B}}$ is extracted which amounts to 910 K. In addition, if a Boltzmann-like

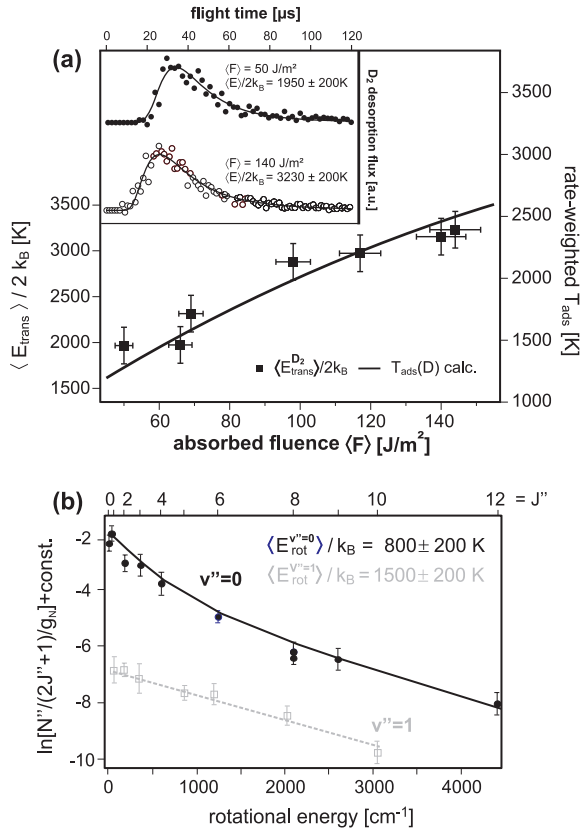

Figure 16. Energy partitioning in the fs-laser-induced associative hydrogen desorption from Ru(001). (a) Mean translational energies $\langle E_{\mathrm{trans}}\rangle/2k_{\mathrm{B}}$ (left axis) of the desorbing D_2 molecules derived from TOF spectra (see inset) as a function of the adsorbed laser fluence $\langle F\rangle$. Solid lines represent an averaged adsorbate temperature $T_{\mathrm{ads}}^{\mathrm{RW}}$ (right axis), see text. Note the qualitative agreement despite a scaling factor between both axes. (b) Rotational population for the vibrational ground and first excited state of the desorbing D_2 molecules ($\langle F\rangle = 85$ J m^{-2}) obtained by state-resolved detection based on the REMPI technique. Panel (b) reprinted with permission from [58]. Copyright 2005 American Physical Society.

vibrational distribution is assumed for both states ($v = 0$ and 1) detected in the experiment, a vibrational temperature of T_{vib} of 1200 K is derived. With these values for T_{rot} and T_{vib} and the respective translational temperature $T_{\mathrm{trans}} = E_{\mathrm{trans}}/2k_{\mathrm{B}} = 2500$ K at the same $\langle F\rangle = 85$ J m^{-2}, one may then establish a total energy balance according to $E_{\mathrm{D_2}}^{\mathrm{flux}} = 2k_{\mathrm{B}}T_{\mathrm{trans}} + k_{\mathrm{B}}T_{\mathrm{rot}} + k_{\mathrm{B}}T_{\mathrm{vib}}$ [76]. The factor of 2 in the term for the translational contribution originates from the density-to-flux conversion of the TOF spectra measured by a QMS, since one has to account for the particle-velocity-dependent ionization probability of the mass detector [77]. Comparison of $E_{\mathrm{D_2}}^{\mathrm{flux}}$ with the energy content of the adsorbate layer $E_{\mathrm{ads}} = 4k_{\mathrm{B}}T_{\mathrm{ads}}$ at equilibrium conditions with all temperatures equal yields an experimental value for T_{ads} of 1780 K. This is in excellent agreement with the calculated rate-weighted adsorbate temperature $T_{\mathrm{ads}}^{\mathrm{RW}} = 1810$ K. Given that in the electronic friction model, which is used in these calculations, one assumes a constant and one-dimensional friction coefficient together with a single adsorbate temperature which uniformly characterizes the adlayer, these results of the energy balancing appear rather astonishing.

The experimental facts are, however, that energy partitioning in the hydrogen recombination is significantly different for the various degrees of freedom. The energy contents in translational, vibrational and rotational degrees approximately scale as 5.4:1.3:1. This obvious preference for translational excitation of the reaction product could, in principle, originate from two contributions. (i) In the case that the ground state PES governs the reaction dynamics, the location of a possible reaction barrier crucially influences the energy partitioning as mentioned before. (ii) A multidimensional frictional coupling to the hot-electron distribution might also account for the unequal energy transfer between different degrees of freedom of the reaction product. In other words, a faster and preferential energy flow into the height coordinate z between the adsorbate and substrate versus the interatomic-distance coordinate d could also explain the enhanced translational energy of the desorbing D_2 molecules as seen in the experiment. In the final subsection on the femtochemistry of H/Ru(001) reviewed in this paper, multidimensional dynamics calculations on this system will be discussed in more detail to address the observed unequal energy partitioning.

Additional information on the molecular motion of the nascent D_2 molecules is obtained by varying the polarization of the resonant excitation. All REMPI schemes exploiting one-photon transitions in the resonant excitation step, i.e. all $(1+x)$ excitation schemes, allow for obtaining information on the molecular alignment of the desorbing particles. Here, the molecular polarization $P = (I_\parallel - I_\perp)/(I_\parallel + I_\perp)$ is measured where $I_\parallel$ and $I_\perp$ denote the ion intensity obtained for parallel, respectively perpendicular, laser polarization of the resonant excitation step with respect to the surface normal [59]. The rotational alignment factor $-1 \leqslant A_0^{(2)} \leqslant 2$ inferred from P generally depends on the rotational branch [78] and describes the preferential motion while the desorbing molecule leaves the surface. A positive $A_0^{(2)}$ implies a preference for a helicopter-like rotation, whereas $A_0^{(2)} < 0$ indicates a more cartwheel-like motion [58, 59, 78]. The alignment measurements on the D/Ru(001) system, the only ones of their kind for an fs-laser-induced desorption reaction, yield a substantial, but laser fluence and quantum-state-independent positive alignment ($A_0^{(2)} = 0.27$), which means that a predominantly helicopter-like motion is involved in the molecular motion of the departing D_2 from the Ru surface.

4.4. Multidimensional dynamics

The quantitative description of nonadiabatic coupling between the substrate and the adsorbate via (electronic) friction (as outlined in section 2.2) was originally developed to describe fs-laser-induced desorption of diatomic molecules along the centre-of-mass coordinate, which can be reduced to a one-dimensional (1D) problem [44, 45]. Thus, it is not clear *a priori* why such a 1D model should be appropriate for an associative desorption reaction, since this process has to be viewed at least as a two-dimensional (2D) problem comprising the interatomic distance, i.e. the bond length d and the distance z of the centre of the diatomic product molecule from the surface. Nonetheless, the 1D model has been applied with (almost surprisingly) great success also to association reactions like the CO + O oxidation on Ru(001) [15] and—as demonstrated above—the H + H recombination on the same surface. See the two-pulse correlation, fluence dependence, isotope effect, etc, of the hydrogen/ruthenium system in the previous subsections. After a first successful application of frictional coupling along *two* dimensions to the H_2/Cu(111) and N_2/Ru(001) by Luntz and Persson [52], the same concept has also been applied to the H/Ru(001) system [53]. Here, a three-dimensional (3D) model is introduced with two coordinates d and z representing the nascent hydrogen molecule (see figure 17(b)), whereas the third dimension with a single phonon coordinate q describes the coupling to the Ru lattice by dynamic recoil. Both the potential energy surface and the electronic friction tensor are calculated by density functional theory (DFT) [52, 53] so that there are no adjustable parameters in the comparison of this model with the wide range of experimental data available for the H/Ru(001) system. Based on the molecular dynamics with electronic friction by Head-Gordon and Tully [51], the 3D classical equations of motion on the PES $V(z, d, q)$ are given by

$$\mu\ddot{d} = -\frac{\partial V}{\partial d} - \gamma_{dd}\dot{d} - \gamma_{dz}\dot{z} + F_d(t) \tag{12}$$

$$m\ddot{z} = -\frac{\partial V}{\partial z} - \gamma_{zz}\dot{z} - \gamma_{dz}\dot{d} + F_z(t) \tag{13}$$

$$M_s\ddot{q} = -\frac{\partial V}{\partial q} - \gamma_q\dot{q} + F_q(t), \tag{14}$$

where μ, m and M_s are the reduced mass of the vibration, the molecular mass and the surface mass of an Ru atom, respectively. The molecular modes z and d are coupled to a thermalized electron distribution at temperature T_{el} via the frictional tensor γ_{ij} which causes damping and induces fluctuating forces $F_i(t)$, $(i = z, d)$ according to the second fluctuation-dissipation theorem [79]:

$$\langle F_i(t)F_i(t')\rangle = 2k_B T_{el}\gamma_{ii}\delta(t - t'). \tag{15}$$

Equation (15) and the analog version for the phonon coordinate q relate the transient electronic and phononic temperatures $T_{el}(t)$ and $T_{ph}(t)$ obtained from the 2TM to the forces driving the molecular dynamics of the photodesorption process.

Figure 17(a) shows the calculated frictional tensor elements γ_{ij}, which are plotted along the minimum energy path S towards desorption. The frictional coefficients for the different coordinates are largely similar at $S = 0$, the position on the PES which corresponds to the initially adsorbed state where both hydrogen atoms reside on the Ru surface in equilibrium before the laser excitation occurs. In contrast, near the transition state V^* at $S \approx 2$ Å, $3\gamma_{dd} \approx \gamma_{zz}$. In addition, the 2D PES $V(z, d, q = 0)$ of the H[1 × 1]/Ru(001) ground state is obtained also by DFT calculations using a 2 × 2 (and partially 4 × 4) Ru unit cells for desorption of a single H_2 molecule. Depending on the excitation density, i.e. laser fluence, and hence the desorption probability, classical trajectories are run for this system in molecular dynamics calculations. In

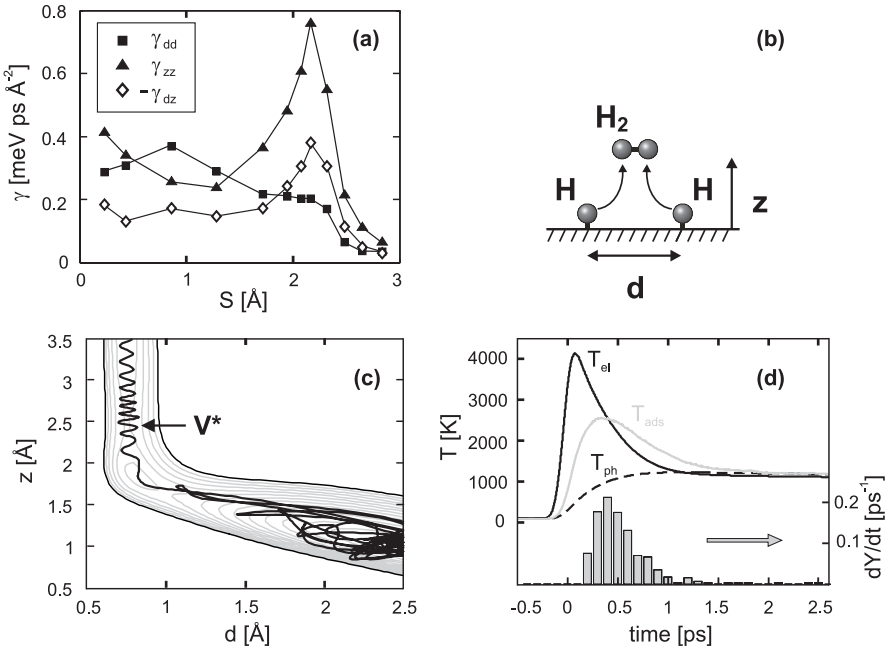

Figure 17. DFT and molecular dynamics calculations for the fs-laser-induced associative desorption of H_2 from Ru(001). (a) Multidimensional friction coefficients γ_{ij} along the minimum energy pathway S, where $S = 0$ Å corresponds to the adsorbed state, $[1 \times 1]$H/Ru(001) before excitation, and $S = 3$ Å to the $H_2 + H$/Ru(001) asymptote. Panel (b) illustrates the associative desorption process with d the interatomic distance and z the distance between the centre of mass of the nascent H–H molecule and the Ru surface. (c) Contour plot of the 2D potential energy surface $V(z, d)$ with 0.1 eV energy intervals. The barrier in the desorption exit channel is marked by V^*. A typical associative H_2 desorption trajectory following fs-laser excitation of 140 J m^{-2} adsorbed fluence is overlaid. (d) Transients of electron and phonon temperature T_{el} and T_{ph}, respectively, obtained with the two-temperature model together with the time-dependent adsorbate temperature $T_{ads} = E_{H_2}/2k_B$ and the H_2 desorption rate $dY(t)/dt$ (bar graph). Note that the electronic temperature has already significantly decreased by the time the nascent H_2 reaches the transition state at $S \approx 2$ Å. As a consequence, the significant differences in γ near that portion of the PES might play only a secondary role in the energy transfer from the substrate to the adsorbate. Furthermore, rapid intermixing of the z and d coordinates is observed while the H–H climbs out of the adsorption well. Reprinted with permission from [53]. Copyright 2006 American Institute of Physics.

figure 17(c), an exemplary trajectory of two H atoms forming a H–H complex, which then leaves the surface in an successful desorption event, is overlaid onto the 2D contour plot of the calculated PES. By evaluating an appropriate number of such desorption trajectories, most of the experimental results could be reproduced with remarkably good agreement: the two-pulse correlation, the nonlinear fluence dependence of the desorption yield and the isotope effect [53].

Analysing individual trajectories (like the one of figure 17(c)) reveals the following intriguing conclusion: most of the primary electron-mediated excitation of nuclear coordinates occurs during or shortly after the laser pulse when the system is still deep in the H–H adsorption well and much below the reaction barrier. In this region, although $\gamma_{dd} \approx \gamma_{zz}$, most of the nuclear excitation occurs through the vibrational coordinate because of the four times smaller reduced mass along the coordinate d versus that along z [53]. By the time the H–H approaches the barrier where $\gamma_{zz} \gg \gamma_{dd}$, the electron temperature T_{el} has already cooled down so that the frictional force F_i is small (see figure 17(d)). However, even though initially most of the excitation occurs through the vibrational coordinate, the rapid energy exchange, i.e. 'thermalization', between the d and the z coordinate along the trajectory conserves little memory of the mode of excitation. Hence the observed differences in the energy partition between translational and vibrational degrees of freedom originate predominantly from the topology of the ground state PES. In particular, the small but distinct barrier in the translational channel plays a crucial role for the excess energy in the translational degree of freedom.

However, one significant difference between the 1D model and the 3D dynamics is that the 1D model assumes that whenever the total energy associated with the desorbing H_2 molecule is larger than the barrier height, $E_{H_2} > V^*$, that desorption occurs. But this is no longer true in multidimensional dynamics, since a forming H–H will not successfully desorb as an H_2 molecule if it does not experience adequate excitation leading to proper motion on the ground state PES which governs the desorption dynamics. In other words, phase space arguments apply when, despite sufficient energy to overcome the barrier, a particular H–H trajectory does not lead to associative desorption. As a consequence, when the results of the 3D trajectories are projected onto 1D, fluence (adsorbate temperature) dependent phase space constraints in multidimensional dynamics look approximately like an additional barrier $\exp[-\Delta V^*/(k_B T_{ads})]$ that adds to the true energy for desorption E_a [53]. This is probably the reason that the fit of the 1D model to the H_2/Ru(001) experiments requires an E_a greater than observed experimentally in thermal desorption (see above $E_{ads} =$

1.35 eV obtained with the 1D friction calculation in section 2.2 as compared to the TDS value for E_a of ∼1.0 eV [70]). Although phase space may not be populated in a completely statistical manner during the short time of the fs-laser-induced chemistry, the origin of the phase space barrier is similar to the temperature-dependent 'entropic barrier' in transition state theory so that the true barrier is that associated with the free energy. In terms of this analogy, it may be argued that the phase space or entropic barriers in femtochemistry will be small for loose transition states (e.g. molecular desorption) but larger for tighter transition states (e.g. surface diffusion, association reactions). Consequently, some caution should be used in interpreting activation energies obtained from fitting experiments to the one-dimensional model [53].

5. Concluding remarks

The current review has given an overview over the concepts of ultrafast laser-induced surface reactions on a metal substrate and how the evolving reaction dynamics are experimentally investigated and theoretically modelled. The results for the prototype of such a surface reaction, namely the associative hydrogen desorption from Ru(001) $H_{ads} + H_{ads} \rightarrow H_{2,gas}$/Ru(001), obtained over the past few years have then been discussed in detail: the experimental findings of an ultrafast, hot-substrate electron-mediated reaction pathway, significant adsorbate–adsorbate interactions as manifested in dynamic promotion effects as well as in a clear coverage threshold for successful desorption and finally energy partitioning between different degrees of freedom with preferentially translational excitation of the reaction product provide a comprehensive understanding of many microscopic aspects of this reaction. Multidimensional friction calculations reveal that initially energy is transferred to nuclear motion by nonadiabatic coupling, but that subsequently the ground state potential energy surface governs the ultrafast reaction dynamics of the H_2 recombination. The rapid energy exchange between different modes of the nascent H_2 molecule is the origin of the remarkable success of the usually applied one-dimensional friction model in describing this inherently multidimensional reaction of H_2 association.

One has to keep in mind that this specific reaction system, H_2 on Ru(001), serves as the model system for understanding elementary physical and chemical aspects of surface reactions. The light mass of the reactants enables one to observe fundamental effects in a very pronounced fashion like the very short adsorbate–substrate coupling times or the drastic isotope effect (due to the large mass ratio between H and D). Also certain characteristics of the metal substrate ruthenium, like the strong electron–phonon coupling, contribute to clearly differentiate electron- from phonon-mediated reaction mechanisms. However, beyond these issues of model character of H/Ru, a recent report on syngas ($CO + H_2$) reactions [80] might also indicate a broader and application-oriented relevance of hydrogen reaction dynamics as reviewed here. In that study, Gerber and coworkers showed for various syngas mixtures streaming over a Pd(100) single crystal how different bond-forming reaction pathways could be optimized using tailored ultrashort laser pulses.

Exactly this desire to control the efficiency and selectivity of specific reaction channels by light represents one of the major challenges of chemical reaction dynamics in general and also in particular at surfaces [8]. However, since at metals the electronic excitation step is substrate-mediated and indirect, a coherent control scenario is evidently not as straightforward as in the gas or solution phase [81–84]. This originates from the ultrashort timescales of competing dephasing and energy relaxation processes for reactants adsorbed on metal surfaces, which leads to a rapid loss of electronic and vibrational coherence. One approach to still accomplish some control of the reaction yield is to vibrationally pre-excite the adsorbed reactants by an intense IR pulse prior to the electronic excitation which eventually triggers the desired reaction. On the experimental side, the only successful example for selectively exciting and breaking an adsorbate–substrate bond by IR photons without rapid thermalization due to vibrational energy redistribution is the FEL (free electron laser)-based work by Liu *et al* [85] on the associative H_2 desorption from H/Si(111). The mode selectivity, which is achieved in this particular surface reaction, benefits from the relatively long vibrational lifetimes (in the ns range) in the ground electronic state.

Application, however, of such a control strategy to strongly coupled, chemisorbed systems like the H/Ru(001) with much shorter vibrational lifetimes (in the sub-ps range) is *a priori* non-trivial. Yet in a recent theoretical study, Vazhappilly *et al* [63] successfully showed that, in a so-called 'hybrid scheme', a direct and controllable IR pulse prepares the system in a coherent manner before the subsequent UV or VIS pulse initiates the photoreaction and applied this control scheme to the associative photodesorption of molecular hydrogen from Ru(001). Open-system density matrix theory [86] is used in a two-state DIET model to calculate the desorption yield enhancement for the H(D)/Ru system after selective excitation of the interatomic-distance mode (d mode) and the adsorbate–substrate distance mode (z mode) with fundamental vibrational energies of $\hbar\omega_d = 94$ meV and $\hbar\omega_z = 136$ meV, respectively. Indeed, bond-selective IR excitation seems possible whereby the z mode can be significantly more easily excited than the d mode due to the one order of magnitude larger transition dipole moment. Using vibrational eigenstates as initially pre-excited states, yield enhancements by a factor of approximately 5 to 15 are found, however, at IR fluences of several J m^{-2}. But fluences more realistically available in the experiment based on table-top laser systems at the corresponding wavelengths of $\lambda_d = 13.2$, μm and $\lambda_z = 9.1$ μm result in an desorption yield increase by only ∼10% [87]. Thus the experimental realization of reaction control of the H_2 desorption from Ru via IR pre-excitation critically depends on the availability of sufficiently high IR fluences, potentially with FELs.

Challenges for the theory side of the H/Ru(001) system finally comprise the quantitative description of the pronounced adsorbate–adsorbate interaction observed in the experiment, the peculiar dynamic promotion effect and the

coverage threshold for fs-laser-induced recombination of the H reactants. Nevertheless, the $H_{ads} + H_{ads} \rightarrow H_{2,gas}$ associative desorption from Ru(001) represents one of the experimentally best studied and theoretically well-modelled surface reactions induced by ultrafast laser excitation.

Acknowledgments

Many thanks go to M Wolf and G Ertl for helpful discussions and support during the different phases of the hydrogen recombination project. The actual experiments reported in this review were carried out by D Denzler, S Wagner, M Rutkowski and in the early stage also by C Hess. I thank them for their diligent and persistent work and long hours in the lab. The successful collaborations with H Zacharias on the state-selective hydrogen detection and with A C Luntz and M Persson on the multidimensional description of the reaction dynamics are gratefully acknowledged. Finally, financial support from the Deutsche Forschungsgemeinschaft (DFG), in particular through Sfb450, has been highly appreciated.

References

[1] Lichtman D and Shapira Y 1978 *CRC Crit. Rev. Solid State Mater. Sci.* **8** 93
[2] Zhou X L, Zhu X Y and White J M 1991 *Surf. Sci. Rep.* **13** 73
[3] Zimmermann F M and Ho W 1995 *Surf. Sci. Rep.* **22** 127
[4] Ramsier R D and Yates R T 1991 *Surf. Sci. Rep.* **12** 243
[5] Prybyla J A, Heinz T F, Misewich J A, Loy M T T and Glownia J H 1990 *Phys. Rev. Lett.* **64** 1537
[6] Budde F, Heinz T F, Loy M M T, Misewich J A, de Rougemont F and Zacharias H 1991 *Phys. Rev. Lett.* **66** 3024
[7] Cavanagh R R, King D S, Stephenson J C and Heinz T F 1993 *J. Chem. Phys.* **97** 786
[8] Frischkorn C and Wolf M 2006 *Chem. Rev.* **106** 4207
[9] Anisimov S I, Kapeliovich B L and Perel'man T L 1974 *Sov. Phys.—JETP* **39** 375
[10] Misewich J A, Kalamarides A, Heinz T F, Höfer U and Loy M M T 1994 *J. Chem. Phys.* **100** 736
[11] Stépán K, Güdde J and Höfer U 2005 *Phys. Rev. Lett.* **94** 236103
[12] Backus E H G, Eichler A, Kleyn A W and Bonn M 2005 *Science* **310** 1790
[13] Kao F J, Busch D G, da Costa D G and Ho W 1993 *Phys. Rev. Lett.* **70** 4098
[14] Her T H, Finlay R J, Wu C and Mazur E 1998 *J. Chem. Phys.* **108** 8595
[15] Bonn M, Funk S, Hess C, Denzler D N, Stampfl C, Scheffler M, Wolf M and Ertl G 1999 *Science* **285** 1042
[16] Denzler D N, Frischkorn C, Wolf M and Ertl G 2004 *J. Phys. Chem.* B **108** 14503
[17] Misewich J A, Heinz T F and Newns D M 1992 *Phys. Rev. Lett.* **68** 3737
[18] Newns D M, Heinz T F and Misewich J A 1991 *Prog. Theor. Phys. Suppl.* **106** 411
[19] Denzler D N, Frischkorn C, Hess C, Wolf M and Ertl G 2003 *Phys. Rev. Lett.* **91** 226102
[20] Persson B N J and Persson M 1980 *Solid State Commun.* **36** 175
[21] Ho W 2002 *J. Chem. Phys.* **117** 11033
[22] Hla S W and Rieder K H 2003 *Annu. Rev. Phys. Chem.* **54** 307
[23] Nienhaus H 2002 *Surf. Sci. Rep.* **45** 1
[24] Wodtke A M, Tully J C and Auerbach D J 2004 *Int. Rev. Phys. Chem.* **23** 513
[25] Denzler D N, Hess C, Funk S, Ertl G, Bonn M, Frischkorn C and Wolf M 2002 *Femtochemistry and Femtobiology* ed A Douhal and J Santamaria (Singapore: World Scientific) p 652
[26] Ertl G, Knözinger H and Weitkamp J (ed) 1997 *Handbook of Heterogeneous Catalysis* (Weinheim: VCH)
[27] de Walle C G V and Neugebauer J 2003 *Nature* **423** 626
[28] Christmann K 1995 *Prog. Surf. Sci.* **48** 15
[29] Somorjai G A 2002 *J. Phys. Chem.* B **106** 9201
[30] Christmann K 1988 *Surf. Sci. Rep.* **9** 1
[31] Mate C M and Somorjai G A 1986 *Phys. Rev.* B **34** 7417
[32] Takagi N, Yasui Y, Takaoka T, Sawada M, Yanagita H, Aruga T and Nishijima M 1996 *Phys. Rev.* B **53** 13767
[33] Kaganov M I, Lifshitz I M and Tanatarov L V 1957 *Sov. Phys.—JETP* **4** 173
[34] Funk S, Bonn M, Denzler D N, Hess C, Wolf M and Ertl G 2000 *J. Chem. Phys.* **112** 9888
[35] Hohlfeld J, Wellershoff S S, Güdde J, Conrad U, Jähnke V and Matthias E 2000 *Chem. Phys.* **251** 237
[36] Lisowski M, Loukakos P A, Bovensiepen U, Stähler J, Gahl C and Wolf M 2004 *Appl. Phys.* A **78** 165
[37] Kittel C 2005 *Introduction to Solid State Physics* (New York: Wiley)
[38] Schober H and Dederrichs P H 1981 *Landolt Börnstein New Series* (Berlin: Springer) p 130
[39] Bonn M, Denzler D N, Funk S, Wolf M, Wellershoff S S and Hohlfeld J 2000 *Phys. Rev.* B **61** 1101
[40] Weaver J H, Krafka C, Lynch D W and Koch E E 1981 *Physical Data—Optical Properties of Metals* (Karlsruhe: Fachinformationszentrum Karlsruhe)
[41] Menzel D and Gomer R 1964 *J. Chem. Phys.* **41** 3311
[42] Redhead P A 1964 *Can. J. Phys.* **42** 886
[43] Antoniewicz P R 1980 *Phys. Rev.* B **21** 3811
[44] Budde F, Heinz T F, Kalamarides A, Loy M M T and Misewich J A 1993 *Surf. Sci.* **283** 143
[45] Brandbyge M, Hedegard P, Heinz T F, Misewich J A and Newns D M 1995 *Phys. Rev.* B **52** 6042
[46] Tully J C, Gomez M and Head-Gordon M 1993 *J. Vac. Sci. Technol.* A **11** 1914
[47] Newns D M 1969 *Phys. Rev.* **178** 1123
[48] Tully J C 1976 *Dynamics in Molecular Collisions* vol B ed W H Miller (New York: Plenum) p 217
[49] Darling G R and Holloway S 1995 *Rep. Prog. Phys.* **58** 1595
[50] Struck L M, Richter L J, Buntin S A, Cavanagh R R and Stephenson J C 1996 *Phys. Rev. Lett.* **77** 4576
[51] Head-Gordon M and Tully J C 1995 *J. Chem. Phys.* **103** 10137
[52] Luntz A C and Persson M 2005 *J. Chem. Phys.* **123** 074704
[53] Luntz A C, Persson M, Wagner S, Frischkorn C and Wolf M 2006 *J. Chem. Phys.* **124** 244702
[54] Groenveld R H M, Sprik R and Lagendijk A 1995 *Phys. Rev.* B **51** 11433
[55] Denzler D N 1999 Untersuchungen zur Ultrakurzzeitdynamik photostimulierter Oberflächenreaktionen und der Energierelaxation in Metallen *Diploma Thesis* Freie Universität Berlin, Physics Department
[56] Feulner P and Menzel D 1980 *J. Vac. Sci. Technol.* **17** 662
[57] Kao F J, Busch D G, Cohen D, da Costa D G and Ho W 1993 *Phys. Rev. Lett.* **71** 2094
[58] Wagner S, Frischkorn C, Wolf M, Rutkowski M, Zacharias H and Luntz A C 2005 *Phys. Rev.* B **72** 205404
[59] Wetzig D, Rutkowski M, Zacharias H and Groß A 2001 *Phys. Rev.* B **63** 205412
[60] Richter L J, Petralli-Mallow T P and Stephenson J C 1998 *Opt. Lett.* **23** 1594
[61] Bonn M, Hess C, Funk S, Miners J H, Persson B N J, Wolf M and Ertl G 2000 *Phys. Rev. Lett.* **84** 4653
[62] Frischkorn C, Wolf M, Höfer U, Güdde J, Saalfrank P, Nest M, Klamroth T, Willig F, Ernstorfer R, Gundlach L, May V, Wang L, Duncan W and Prezhdo O 2007 *Analysis and*

Control of Ultrafast Photoinduced Reactions ed O Kühn and L Wöste (Heidelberg: Springer) p 387
[63] Vazhappilly T, Beyvers S, Klamroth T, Luppi M and Saalfrank P 2007 *Chem. Phys.* **338** 299
[64] Yada M and Madix R J 1995 *Surf. Sci.* **328** 171
[65] King D A and Woodruff D P (ed) 1993 *The Chemical Physics of Solid Surfaces* vol 6 *Coadsorption, Promoters and Poisons* (Amsterdam: Elsevier)
[66] Bird D 1998 *Faraday Discuss.* **110** 335
[67] Hammer B and Norskov J 2000 *Adv. Catal.* **45** 71
[68] Frischkorn C 2005 *Surf. Sci.* **593** 67
[69] Klamroth T and Saalfrank P 2006 private communication
[70] Feulner P and Menzel D 1985 *Surf. Sci.* **154** 465
[71] Lindroos M, Pfnür H and Menzel D 1987 *Surf. Sci.* **192** 421
[72] Greuter F, Strathy I, Plummer E W and Eberhardt W 1986 *Phys. Rev.* B **33** 736
[73] Mitsui T, Rose M K, Fomin E, Ogletree D F and Salmeron M 2003 *Nature* **422** 705
[74] Eyring H and Polanyi M 1931 *Z. Phys. Chem.* B **12** 279
[75] Diekhöner L, Hornekaer L, Mortensen H, Jensen E, Baurichter A, Petrunin V V and Luntz A C 2002 *J. Chem. Phys.* **117** 5018
[76] Kolasinski K W, Nessler W, de Meijere A and Hasselbrink E 1994 *Phys. Rev. Lett.* **72** 1356
[77] Hasselbrink E 1995 *Laser Spectroscopy and Photochemistry on Metal Surfaces* ed H L Dai and W Ho (Singapore: World Scientific) p 685
[78] Greene C H and Zare R N 1982 *Annu. Rev. Phys. Chem.* **33** 119
[79] Tully J C 1995 *J. Chem. Phys.* **73** 1975
[80] Nuernberger P, Wolpert D, Weiss H and Gerber G 2007 *Ultrafast Phenomena* ed P Corkum, D Jonas, R J D Miller and A M Weiner (Berlin: Springer) p 237
[81] Assion A, Baumert T, Bergt M, Brixner T, Kiefer B, Seyfried V, Strehle M and Gerber G 1998 *Science* **282** 919
[82] Rabitz H, de Vievie-Riedle R, Motzkus M and Kompa K 2000 *Science* **288** 824
[83] Brixner T, Damrauer N H, Niklaus P and Gerber G 2001 *Nature* **414** 57
[84] Daniel C, Full J, González L, Lupulescu C, Manz J, Merli A, Vajda S and Wöste L 2003 *Science* **299** 536
[85] Liu Z, Feldman L C, Tolk N H, Zhang Z and Cohen P I 2006 *Science* **312** 1024
[86] Saalfrank P and Kosloff R 1996 *J. Chem. Phys.* **105** 2441
[87] Saalfrank P 2008 private communication